Quasi-consistent efficient meshfree thin shell formulation with naturally stabilized enforced essential boundary conditions

Junchao Wu[a,*], Yangtao Xu[a], Bin Xu[a], Syed Humayun Basha[a]

[a]*Key Laboratory for Intelligent Infrastructure and Monitoring of Fujian Province, Key Laboratory for Structural Engineering and Disaster Prevention of Fujian Province, College of Civil Engineering, Huaqiao University, Xiamen, Fujian, 361021, China*

Abstract

This research proposed an efficient and quasi-consistent meshfree thin shell formulation with naturally stabilized enforcement of essential boundary conditions. Within the framework of the Hu-Washizu variational principle, a mixed formulation of displacements, strains and stresses is employed in this approach, where the displacements are discretized using meshfree shape functions, and the strains and stresses are expressed using smoothed gradients and covariant bases. The smoothed gradients satisfy the first second-order integration constraint and observed variational consistency for polynomial strains and stresses. Owing to Hu-Washizu variational principle, the essential boundary conditions automatically arise in its weak form. As a result, the suggested technique's enforcement of essential boundary conditions resembles that of the traditional Nitsche's method. Contrary to Nitsche's method, the costly higher order derivatives of conventional meshfree shape functions are replaced by the smoothed gradients with fast computation, which improve the efficiency. Meanwhile, the proposed formulation features a naturally stabilized term without adding any artificial stabilization factors, which eliminates the application of penalty method as a stabilization. Further, the efficacy of the proposed Hu-Washizu meshfree thin shell formulation is illustrated by a set of classical standard thin shell problems.

Keywords: Meshfree, Thin shell, Hu-Washizu variational principle, Reproducing kernel gradient smoothing, Essential boundary condition

*Corresponding author
Email address: jcwu@hqu.edu.cn (Junchao Wu)

1. Introduction

Thin shell structures generally adhere to the Kirchhoff hypothesis [1], that neglects the shear deformation can be described using Galerkin formulation which requires to have at least C^1 continuity. Traditional finite element methods typically employ C^0 continuous shape functions, and it prefers hybrid and mixed shell models, like linear and nonlinear Mindlin model [2, 3] and the one inextensible director model [4]. Over the past thirty years, various novel formulations with high order smoothed shape functions have been applied to thin shell formulations. These include element-free Galerkin method [5], maximum-entropy meshfree method [6], Hermite reproducing kernel particle method [7], peridynamics [8], isogeometric analysis [9], and others. For a more comprehensive review of advances and applications of high order formulations in various scientific and engineering fields, refer to [10, 11, 12, 13, 14, 15, 16, 17]. Among these approaches, Galerkin meshfree methods with moving least square approximation (MLS) [18] or reproducing kernel approximation (RK) [19] established the shape functions based on a collection of dispersed nodes, and high order continuity of shape functions can be easily achieved even with low-order basis functions. For thin shell analysis, high order meshfree approximation can also further alleviate the membrane locking caused by the mismatched approximation order of membrane strain and bending strain [5]. Moreover, node-based MLS/RK approximations generally offer the flexibility of local refinement and can relieve the burden of mesh distortion. However, the high order smoothed meshfree shape functions accompany the enlarged and overlapping supports, which may potentially cause many problems for shape functions. One of the issues is the loss of the Kronecker delta property, which means that, unlike the finite element methods, the necessary boundary conditions cannot be directly enforced [20]. Another issue is that the variational consistency or said integration constraint, which is a condition that requires the formulation to exactly reproduce the solution spanned by the basis functions, cannot be satisfied. This issue is mainly caused by the misalignment between the numerical integration domains and supports of shape functions. Thus, the shape functions exhibit a piecewise nature in each integration domain. Besides, it has to be noted that the traditional integration rules like Gauss scheme cannot ensure the integration accuracy in Galerkin weak form [21, 22]. Therefore, variational consistency is vital to the solution accuracy in the Galerkin meshfree formulations.

Various ways have been presented to enforce the necessary boundary for Galerkin meshfree methods directly, including the boundary singular kernel method [23], mixed transformation method [23], and interpolation element-free method [24] for recovering shape functions' Kronecker property. However, these methods were not based on variational setting and cannot guarantee variational consistency. The accuracy maybe poor at locations away from the sample points. In contrast, enforcing the essential boundary conditions using a variational approach is preferred for Galerkin meshfree methods. The variational consistent Lagrange multiplier approach was initially used to the Galerkin meshfree method by Belytschko et al. [18]. In this method, the extra degrees of freedom

are used to determine the discretion of Lagrange multiplier. Ivannikov et al. [25] extended this approach to geometrically nonlinear thin shells. Lu et al. [26] suggested the modified variational essential boundary enforcement approach and expressed the Lagrange multiplier by equivalent traction to eliminate the excess degrees of freedom. However, the coercivity of this approach is not always ensured and potentially reduces the accuracy. Zhu and Atluri [27] pioneered the penalty method for meshfree method, making it a straightforward approach to enforce essential boundary conditions via Galerkin weak form. However, the penalty method lacks variational consistency and requires experimental artificial parameters whose optimal value is hard to determine. Fernández-Méndez and Huerta [20] imposed necessary boundary conditions using Nitsche's approach in the meshfree formulation. This approach can be seen as a hybrid combination of the modified variational method and the penalty method because the modified variational method generates variational consistency through the use of a consistent term, and the penalty method is used as a stabilized term to recover the coercivity. Skatulla and Sansour [28] extended Nitsche's thin shell analysis method and proposed an iteration algorithm to determine artificial parameters at each integration point. Additionally, the Nitsche's method has been successfully applied to maintain the variational consistency between different geometrical or material domains in problems with multiple patches [29] and composite materials [30].

In order to address the issue of numerical integration, a series of consistent integration schemes have been developed for Galerkin meshfree methods. Among these include stabilized conforming nodal integration [31], variational consistent integration [32], quadratic consistent integration [33], reproducing kernel gradient smoothing integration [34], and consistent projection integration [35]. The assumed strain approach establishes the most consistent integration scheme, while the smoothed gradient replaces the costly higher order derivatives of traditional meshfree shape functions and shows a high efficiency. Moreover, to achieve global variational consistency, a consistent essential boundary condition enforcement must be combined with the consistent integration scheme. The combination of consistent integration scheme and Nitsche's method for treating essential boundary conditions may demonstrate better performance since both the methods can satisfy the coercivity without requiring additional degrees of freedom. Nevertheless, Nitsche's approach still retains the artificial parameters in the stabilized terms, and it is essential to remain cautious of the costly higher order derivatives, particularly for thin plate and thin shell problems. Recently, Wu et al. [36, 37] proposed an efficient and stabilized essential boundary condition enforcement method based upon the Hellinger-Reissner variational principle, where a mixed formulation in Hellinger-Reissner weak form recasts the reproducing kernel gradient smoothing integration. The terms required for enforcing essential boundary conditions are identical to the Nitsche's method, and both have consistent and stabilized terms. However, the stabilized term of this method naturally exists in the Hellinger-Reissner weak form and no longer needs the artificial parameters, even for essential boundary enforcement. Instead all of the higher order derivatives are represented by the smoothed gradients and

their derivatives.

In this study, an efficient and stabilized variational consistent meshfree method that naturally enforces the essential boundary conditions is developed for thin shell structures. Following the concept of the Hellinger-Reissner principle base consistent meshfree method, the Hu-Washizu variational principle of complementary energy with variables of displacement, strains, and stresses were employed. The displacement is approximated by conventional meshfree shape functions, and the strains and stresses were expressed by smoothed gradients with covariant bases. It is important to note that although the first second-order integration requirements were naturally embedded in the smoothed gradients, their fulfillment resulted in a quasi-satisfaction of variational consistency. This is mainly because of the non-polynomial nature of the stresses. Hu-Washizu's weak form was used to evaluate all the essential boundary conditions regarding displacements and rotations. This type of formulation is similar to the Nitsche's method but does not require any artificial parameters. Compared with Nitsche's method, conventional reproducing smoothed gradients and its direct derivatives replace the costly higher order derivatives. By utilizing the advantages of a replicating kernel gradient smoothing framework, the smoothed gradients showed better performance compared to conventional derivatives of shape functions, hence increasing the meshfree formulation's computational efficiency.

The remainder of this research article is structured as follows: The kinematics of the thin shell structure and the weak form of the associated Hu-Washizu principle are briefly described in Section 2. The mixed formulation regarding the displacements, strains and stresses in accordance with Hu-Washizu weak form are presented in Section 3. The discrete equilibrium equations are derived in Section 4 using the naturally occurring accommodation of essential. Subsequently, they are compared to the equations obtained using Nitsche's method. The numerical results in Section 5 validate the efficacy of the proposed Hu-Washizu meshfree thin shell formulation. Lastly, the concluding remarks are presented in Section 6.

2. Hu-Washizu's formulation of complementary energy for thin shell

2.1. Kinematics for thin shell

Consider the configuration of a shell $\bar{\Omega}$, as shown in Fig. 1, which can be easily described by a parametric curvilinear coordinate system $\boldsymbol{\xi} = \{\xi^i\}_{i=1,2,3}$. The mid-surface of the shell denoted by Ω is specified by the in-plane coordinates $\boldsymbol{\xi} = \{\xi^\alpha\}_{\alpha=1,2}$, as the thickness direction of shell is by ξ^3, $-\frac{h}{2} \leq \xi^3 \leq \frac{h}{2}$, h is the thickness of shell. In this work, Latin indices take the values from 1 to 3, and Greek indices are evaluated by 1 or 2. For the Kirchhoff hypothesis [5], the position $\boldsymbol{x} \in \bar{\Omega}$ is defined by linear functions with respect to ξ^3 :

$$\boldsymbol{x}(\xi^1, \xi^2, \xi^3) = \boldsymbol{r}(\xi^1, \xi^2) + \xi^3 \boldsymbol{a}_3(\xi^1, \xi^2) \tag{1}$$

in which $\boldsymbol{r}$ means the position on the mid-surface of shell, and $\boldsymbol{a}_3$ is corresponding normal direction. For the mid-surface of shell, the in-plane covariant base vector with respect to ξ^α can be derived by a trivial partial differentiation to $\boldsymbol{r}$:

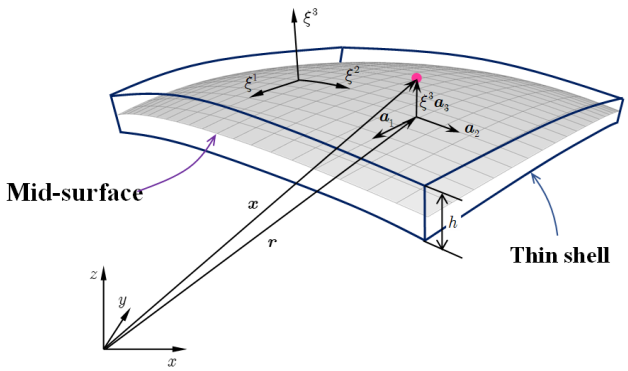

Figure 1: Kinematics for thin shell.

$$\boldsymbol{a}_\alpha = \frac{\partial \boldsymbol{r}}{\partial \xi^\alpha} = \boldsymbol{r}_{,\alpha}, \alpha = 1, 2 \tag{2}$$

to provide for a clear expression, the subscript comma denotes the partial differentiation operation with respect to in-plane coordinates ξ^α, and the normal vector $\boldsymbol{a}_3$ can be obtained by the normalized cross product of $\boldsymbol{a}_\alpha$'s as follows:

$$\boldsymbol{a}_3 = \frac{\boldsymbol{a}_1 \times \boldsymbol{a}_2}{\|\boldsymbol{a}_1 \times \boldsymbol{a}_2\|} \tag{3}$$

where $\| \bullet \|$ is the Euclidean norm operator.

With the assumption of infinitesimal deformation, the strain components with respect to the global contravariant base can be stated as:

$$\epsilon_{ij} = \frac{1}{2}(\boldsymbol{x}_{,i} \cdot \boldsymbol{u}_{,j} + \boldsymbol{u}_{,i} \cdot \boldsymbol{x}_{,j}) \tag{4}$$

where $\boldsymbol{u}$ represents the displacement for the shell deformation. To satisfy the Kirchhoff hypothesis, the displacement is assumed to be of the following form:

$$\boldsymbol{u}(\xi^1,\xi^2,\xi^3) = \boldsymbol{v}(\xi^1,\xi^2) + \boldsymbol{\theta}(\xi^1,\xi^2)\xi^3 \tag{5}$$

in which the quadratic and higher order terms are neglected. $\boldsymbol{v}$, $\boldsymbol{\theta}$ resperesent the displacement and rotation in mid-surface, respectively.

Subsequently, plugging Eqs. (1) and (5) into Eq. (4) and neglecting the quadratic terms, the strain components can be rephrased as follows:

$$\begin{aligned}\epsilon_{\alpha\beta} &= \frac{1}{2}(\boldsymbol{a}_\alpha \cdot \boldsymbol{v}_{,\beta} + \boldsymbol{v}_{,\alpha} \cdot \boldsymbol{a}_\beta) \\ &\quad + \frac{1}{2}(\boldsymbol{a}_{3,\alpha} \cdot \boldsymbol{v}_{,\beta} + \boldsymbol{v}_{,\alpha} \cdot \boldsymbol{a}_{3,\beta} + \boldsymbol{a}_\alpha \cdot \boldsymbol{\theta}_{,\beta} + \boldsymbol{\theta}_{,\alpha} \cdot \boldsymbol{a}_\beta)\xi^3 \\ &= \varepsilon_{\alpha\beta} + \kappa_{\alpha\beta}\xi^3\end{aligned} \tag{6a}$$

$$\epsilon_{\alpha 3} = \frac{1}{2}(\boldsymbol{a}_\alpha \cdot \boldsymbol{\theta} + \boldsymbol{v}_{,\alpha} \cdot \boldsymbol{a}_3) + \frac{1}{2}(\boldsymbol{a}_3 \cdot \boldsymbol{\theta})_{,\alpha}\xi^3 \tag{6b}$$

$$\epsilon_{33} = \boldsymbol{a}_3 \cdot \boldsymbol{\theta} \tag{6c}$$

where $\varepsilon_{\alpha\beta}$, $\kappa_{\alpha\beta}$ represent membrane and bending strains, respectively, and are given as follows:

$$\varepsilon_{\alpha\beta} = \frac{1}{2}(\boldsymbol{a}_\alpha \cdot \boldsymbol{v}_{,\beta} + \boldsymbol{v}_{,\alpha} \cdot \boldsymbol{a}_\beta) \tag{7}$$

$$\kappa_{\alpha\beta} = \frac{1}{2}(\boldsymbol{a}_{3,\alpha} \cdot \boldsymbol{v}_{,\beta} + \boldsymbol{v}_{,\alpha} \cdot \boldsymbol{a}_{3,\beta} + \boldsymbol{a}_\alpha \cdot \boldsymbol{\theta}_{,\beta} + \boldsymbol{\theta}_{,\alpha} \cdot \boldsymbol{a}_\beta) \tag{8}$$

In accordance with the Kirchhoff hypothesis, the thickness of shell will not change, and the deformation related with direction of ξ^3 will vanish, i.e. $\epsilon_{3i} = 0$. Thus, the rotation $\boldsymbol{\theta}$ can be rewritten as:

$$\epsilon_{3i} = 0 \Rightarrow \begin{cases} \boldsymbol{\theta} \cdot \boldsymbol{a}_\alpha = -\boldsymbol{v}_{,\alpha} \cdot \boldsymbol{a}_3 \\ \boldsymbol{\theta} \cdot \boldsymbol{a}_3 = 0 \end{cases} \Rightarrow \boldsymbol{\theta} = -\boldsymbol{v}_{,\alpha} \cdot \boldsymbol{a}_3 \boldsymbol{a}^\alpha \tag{9}$$

where $\boldsymbol{a}^\alpha$'s is the in-plane contravariant base vector, $\boldsymbol{a}^\alpha \cdot \boldsymbol{a}_\beta = \delta^\alpha_\beta$, δ is the Kronecker delta function. The detailed derivation of Eq. 9 can be found in [38].

Furthermore, on substituting Eq. (9) into Eq. (8) leads to:

$$\kappa_{\alpha\beta} = (\Gamma^\gamma_{\alpha\beta}\boldsymbol{v}_{,\gamma} - \boldsymbol{v}_{,\alpha\beta}) \cdot \boldsymbol{a}_3 = -\boldsymbol{v}_{,\alpha}|_\beta \cdot \boldsymbol{a}_3 \tag{10}$$

in which $\Gamma^\gamma_{\alpha\beta} = \boldsymbol{a}_{\alpha,\beta} \cdot \boldsymbol{a}^\gamma$ is namely the Christoffel symbol of the second kind, and $\boldsymbol{v}_{,\alpha}|_\beta$ is the in-plane covariant derivative of $\boldsymbol{v}_{,\alpha}$, i.e. $\boldsymbol{v}_{,\alpha}|_\beta = \Gamma^\gamma_{\alpha\beta}\boldsymbol{v}_{,\gamma} - \boldsymbol{v}_{,\alpha\beta}$.

2.2. Galerkin weak form for Hu-Washizu principle of complementary energy

In this study, the Hu-Washizu variational principle of complementary energy [39] was adopted for the development of the proposed analytical approach, the

corresponding complementary functional, denoted by Π_C, is listed as follows:

$$\begin{aligned}
&\Pi_C(\varepsilon_{\alpha\beta}, \kappa_{\alpha\beta}, N^{\alpha\beta}, M^{\alpha\beta}) \\
&= \int_\Omega \frac{h}{2} \varepsilon_{\alpha\beta} C^{\alpha\beta\gamma\eta} \varepsilon_{\gamma\eta} d\Omega + \int_\Omega \frac{h^3}{24} \kappa_{\alpha\beta} C^{\alpha\beta\gamma\eta} \kappa_{\gamma\eta} d\Omega \\
&+ \int_\Omega \varepsilon_{\alpha\beta} (N^{\alpha\beta} - hC^{\alpha\beta\gamma\eta} \varepsilon_{\gamma\eta}) d\Omega + \int_\Omega \kappa_{\alpha\beta} (M^{\alpha\beta} - \frac{h^3}{12} C^{\alpha\beta\gamma\eta} \kappa_{\gamma\eta}) d\Omega \\
&- \int_{\Gamma_v} \boldsymbol{T} \cdot \bar{\boldsymbol{v}} d\Gamma + \int_{\Gamma_\theta} M_{\boldsymbol{nn}} \bar{\theta}_{\boldsymbol{n}} d\Gamma - (P \boldsymbol{a}_3 \cdot \bar{\boldsymbol{v}})_{\boldsymbol{x} \in C_w}
\end{aligned} \tag{11}$$

where $C^{\alpha\beta\gamma\eta}$'s represent the components of fourth order elasticity tensor with respect to the covariant base and plane stress assumption, and it can be expressed by Young's modulus E, Poisson's ratio ν and the in-plane contravariant metric coefficients $a^{\alpha\beta}$'s, $a^{\alpha\beta} = \boldsymbol{a}^\alpha \cdot \boldsymbol{a}^\beta$, as follows:

$$C^{\alpha\beta\gamma\eta} = \frac{E}{2(1+\nu)} (a^{\alpha\gamma} a^{\beta\eta} + a^{\alpha\eta} a^{\beta\gamma} + \frac{2\nu}{1-\nu} a^{\alpha\beta} a^{\gamma\eta}) \tag{12}$$

and $N^{\alpha\beta}$, $M^{\alpha\beta}$ represent the components of membrane- and bending- stresses which are given by:

$$N^{\alpha\beta} = hC^{\alpha\beta\gamma\eta} \varepsilon_{\gamma\eta}, \quad M^{\alpha\beta} = \frac{h^3}{12} C^{\alpha\beta\gamma\eta} \kappa_{\gamma\eta} \tag{13}$$

Essential boundaries on the edges and corners denoted by Γ_v, Γ_θ and C_v are naturally existed in complementary energy functional, and $\bar{\boldsymbol{v}}$, $\bar{\theta}_{\boldsymbol{n}}$ are the corresponding prescribed displacement and normal rotation, respectively. $\boldsymbol{T}$, $M_{\boldsymbol{nn}}$ and P can be determined by Euler-Lagrange equations of shell problem [38] as follows:

$$\boldsymbol{T} = \boldsymbol{T}_N + \boldsymbol{T}_M \ \rightarrow \begin{cases} \boldsymbol{T}_N = \boldsymbol{a}_\alpha N^{\alpha\beta} n_\beta \\ \boldsymbol{T}_M = (\boldsymbol{a}_3 M^{\alpha\beta} s_\alpha n_\beta)_{,\gamma} s^\gamma + (\boldsymbol{a}_3 M^{\alpha\beta})|_\beta n_\alpha \end{cases} \tag{14}$$

$$M_{\boldsymbol{nn}} = M^{\alpha\beta} n_\alpha n_\beta \tag{15}$$

$$P = -[[M^{\alpha\beta} s_\alpha n_\beta]] \tag{16}$$

where $\boldsymbol{n} = n^\alpha \boldsymbol{a}_\alpha = n_\alpha \boldsymbol{a}^\alpha$ and $\boldsymbol{s} = s^\alpha \boldsymbol{a}_\alpha = s_\alpha \boldsymbol{a}^\alpha$ are the outward normal and tangent directions on boundaries. $[[f]]$ is the jump operator defined by:

$$[[f]]_{\boldsymbol{x}=\boldsymbol{x}_c} = \lim_{\boldsymbol{\epsilon} \to \boldsymbol{0}+} (f(\boldsymbol{x}_c + \boldsymbol{\epsilon}) - f(\boldsymbol{x}_c - \boldsymbol{\epsilon})), \boldsymbol{x}_c \in \Gamma \tag{17}$$

where f is an arbitrary function on Γ.

Moreover, the natural boundary conditions should be applied by Lagrangian multiplier method with displacement $\boldsymbol{v}$ regarded as multiplier. Thus, then the

new complementary energy functional namely Π is given by:

$$\begin{aligned}&\Pi(\boldsymbol{v}, \varepsilon_{\alpha\beta}, \kappa_{\alpha\beta}, N^{\alpha\beta}, M^{\alpha\beta})\\ =&\Pi_C(\varepsilon_{\alpha\beta}, \kappa_{\alpha\beta}, N^{\alpha\beta}, M^{\alpha\beta}) + \int_{\Gamma_M} \theta_{\boldsymbol{n}}(M_{\boldsymbol{nn}} - \bar{M}_{\boldsymbol{nn}})d\Gamma\\ -&\int_{\Gamma_T} \boldsymbol{v}\cdot(\boldsymbol{T}-\bar{\boldsymbol{T}})d\Gamma - \boldsymbol{v}\cdot\boldsymbol{a}_3(P-\bar{P})_{\boldsymbol{x}\in C_P} - \int_{\Omega}\boldsymbol{v}\cdot(\boldsymbol{b}-\bar{\boldsymbol{b}})d\Omega\end{aligned} \tag{18}$$

where $\bar{\boldsymbol{T}}$, $\bar{M}_{\boldsymbol{nn}}$ and $\bar{P}$ are the prescribed traction, bending moment and concentrated force on edges Γ_T, Γ_M and corner C_P respectively. All the specified boundaries meet the following geometric relationships:

$$\begin{cases}\Gamma = \Gamma_v \cup \Gamma_T \cup \Gamma_\theta \cup \Gamma_M, \quad C = C_v \cup C_P,\\ \Gamma_v \cap \Gamma_T = \Gamma_\theta \cap \Gamma_M = C_v \cap C_P = \varnothing\end{cases} \tag{19}$$

and $\bar{\boldsymbol{b}}$ stands for the prescribed body force in Ω, $\boldsymbol{b}$ can be written based on Euler-Lagrange equations [38] as:

$$\boldsymbol{b} = \boldsymbol{b}_N + \boldsymbol{b}_M \rightarrow \begin{cases}\boldsymbol{b}_N = (\boldsymbol{a}_\alpha N^{\alpha\beta})|_\beta\\ \boldsymbol{b}_M = (\boldsymbol{a}_3 M^{\alpha\beta})|_{\alpha\beta}\end{cases} \tag{20}$$

Introducing a standard variational argument to Eq. (18), $\delta\Pi = 0$, and considering the arbitrariness of virtual variables, $\delta\boldsymbol{v}$, $\delta\varepsilon_{\alpha\beta}$, $\delta\kappa_{\alpha\beta}$, $N^{\alpha\beta}$, $M^{\alpha\beta}$ lead to the following weak form:

$$-\int_\Omega h\delta\varepsilon_{\alpha\beta}C^{\alpha\beta\gamma\eta}\varepsilon_{\gamma\eta}d\Omega + \int_\Omega \delta\varepsilon_{\alpha\beta}N^{\alpha\beta}d\Omega = 0 \tag{21a}$$

$$-\int_\Omega \frac{h^3}{12}\delta\kappa_{\alpha\beta}C^{\alpha\beta\gamma\eta}\kappa_{\gamma\eta}d\Omega + \int_\Omega \delta\kappa_{\alpha\beta}M^{\alpha\beta}d\Omega = 0 \tag{21b}$$

$$\int_\Omega \delta N^{\alpha\beta}\varepsilon_{\alpha\beta}d\Omega - \int_\Gamma \delta\boldsymbol{T}_N\cdot\boldsymbol{v}d\Gamma + \int_\Omega \delta\boldsymbol{b}_N\cdot\boldsymbol{v}d\Omega + \int_{\Gamma_v}\delta\boldsymbol{T}_N\cdot\boldsymbol{v}d\Gamma = \int_{\Gamma_v}\delta\boldsymbol{T}_N\cdot\bar{\boldsymbol{v}}d\Gamma \tag{21c}$$

$$\begin{aligned}\int_\Omega \delta M^{\alpha\beta}\kappa_{\alpha\beta}d\Omega - \int_\Gamma \delta M_{\boldsymbol{nn}}\theta_{\boldsymbol{n}}d\Gamma + \int_\Gamma \delta\boldsymbol{T}_M\cdot\boldsymbol{v}d\Gamma + (\delta P\boldsymbol{a}_3\cdot\boldsymbol{v})_{\boldsymbol{x}\in C} + \int_\Omega\delta\boldsymbol{b}_M\cdot\boldsymbol{v}d\Omega\\ + \int_{\Gamma_\theta}\delta M_{\boldsymbol{nn}}\theta_{\boldsymbol{n}}d\Gamma - \int_{\Gamma_v}\delta\boldsymbol{T}_M\cdot\boldsymbol{v}d\Gamma - (\delta P\boldsymbol{a}_3\cdot\boldsymbol{v})_{\boldsymbol{x}\in C_v}\\ = \int_{\Gamma_\theta}\delta M_{\boldsymbol{nn}}\bar{\theta}_{\boldsymbol{n}}d\Gamma - \int_{\Gamma_v}\delta\boldsymbol{T}_M\cdot\bar{\boldsymbol{v}}d\Gamma - (\delta P\boldsymbol{a}_3\cdot\bar{\boldsymbol{v}})_{\boldsymbol{x}\in C_v}\end{aligned} \tag{21d}$$

$$\int_{\Gamma} \delta\theta_{\boldsymbol{n}} M_{\boldsymbol{nn}} d\Gamma - \int_{\Gamma} \delta\boldsymbol{v} \cdot \boldsymbol{T} d\Gamma - (\delta\boldsymbol{v} \cdot \boldsymbol{a}_3 P)_{\boldsymbol{x}\in C} + \int_{\Omega} \delta\boldsymbol{v} \cdot \boldsymbol{b} d\Omega$$
$$- \int_{\Gamma_\theta} \delta\theta_{\boldsymbol{n}} M_{\boldsymbol{nn}} d\Gamma + \int_{\Gamma_v} \delta\boldsymbol{v} \cdot \boldsymbol{T} d\Gamma + (\delta\boldsymbol{v} \cdot \boldsymbol{a}_3 P)_{\boldsymbol{x}\in C_v} = - \int_{\Gamma_T} \delta\boldsymbol{v} \cdot \bar{\boldsymbol{t}} d\Gamma - \int_{\Omega} \delta\boldsymbol{v} \cdot \bar{\boldsymbol{b}} d\Omega \tag{21e}$$

where the geometric relationships of Eq. (19) is used herein.

3. Mixed meshfree formulation for modified Hu-Washizu's weak form

3.1. Reproducing kernel approximation for displacement

This study approximates the displacement by adopting reproducing kernel approximation. As shown in Fig. 2, the mid-surface of the shell Ω is discretized by a set of meshfree nodes $\{\boldsymbol{\xi}_I\}_{I=1}^{n_p}$ in parametric configuration, where n_p is the total number of meshfree nodes. The approximated displacement namely $\boldsymbol{v}^h$ can be expressed as:

$$\boldsymbol{v}(\boldsymbol{\xi}) = \sum_{I=1}^{n_p} \Psi_I(\boldsymbol{\xi}) \boldsymbol{d}_I \tag{22}$$

where Ψ_I and $\boldsymbol{d}_I$ represent the shape function and nodal coefficient tensor related by node $\boldsymbol{\xi}_I$. According to reproducing kernel approximation [19], the shape function takes the following form:

$$\Psi_I(\boldsymbol{\xi}) = \boldsymbol{p}^T(\boldsymbol{\xi}) \boldsymbol{c}(\boldsymbol{\xi}) \phi(\boldsymbol{\xi}_I - \boldsymbol{\xi}) \tag{23}$$

where $\boldsymbol{p}$ is the basis function vector represented using the following quadratic function as:

$$\boldsymbol{p} = \{1,\ \xi^1,\ \xi^2,\ (\xi^1)^2, \xi^1\xi^2, (\xi^2)^2\}^T \tag{24}$$

The kernel function denoted by ϕ controls the support and smoothness of meshfree shape functions. The quintic B-spline function with square support is used herein as the kernel function:

$$\phi(\boldsymbol{\xi}_I - \boldsymbol{\xi}) = \phi(\hat{s}_1)\phi(\hat{s}_2), \quad \hat{s}_\alpha = \frac{|\xi_I^\alpha - \xi^\alpha|}{s_{\alpha I}} \tag{25}$$

with

$$\phi(\hat{s}_\alpha) = \frac{1}{5!} \begin{cases} (3 - 3\hat{s}_\alpha)^5 - 6(2 - 3\hat{s}_\alpha)^5 + 15(1 - 3\hat{s}_\alpha)^5 & \hat{s}_\alpha \le \frac{1}{3} \\ (3 - 3\hat{s}_\alpha)^5 - 6(2 - 3\hat{s}_\alpha)^5 & \frac{1}{3} < \hat{s}_\alpha \le \frac{2}{3} \\ (3 - 3\hat{s}_\alpha)^5 & \frac{2}{3} < \hat{s}_\alpha \le 1 \\ 0 & \hat{s}_\alpha > 1 \end{cases} \tag{26}$$

and $s_{\alpha I}$ means the support size of meshfree shape function Ψ_I.

The unknown vector $\boldsymbol{c}$ in shape function are determined by the fulfillment of the so-called consistency condition:

$$\sum_{I=1}^{n_p} \Psi_I(\boldsymbol{\xi}) \boldsymbol{p}(\boldsymbol{\xi}_I) = \boldsymbol{p}(\boldsymbol{\xi}) \tag{27}$$

or equivalently

$$\sum_{I=1}^{n_p} \Psi_I(\boldsymbol{\xi}) \boldsymbol{p}(\boldsymbol{\xi}_I - \boldsymbol{\xi}) = \boldsymbol{p}(\boldsymbol{0}) \tag{28}$$

Substituting Eq. (22) into (28), yields:

$$\boldsymbol{A}(\boldsymbol{\xi}) \boldsymbol{c}(\boldsymbol{\xi}) = \boldsymbol{p}(\boldsymbol{0}) \quad \Rightarrow \quad \boldsymbol{c}(\boldsymbol{\xi}) = \boldsymbol{A}^{-1}(\boldsymbol{\xi}) \boldsymbol{p}(\boldsymbol{0}) \tag{29}$$

where $\boldsymbol{A}$ is the moment matrix:

$$\boldsymbol{A}(\boldsymbol{\xi}) = \sum_{I=1}^{n_p} \phi(\boldsymbol{\xi}_I - \boldsymbol{\xi})\boldsymbol{p}(\boldsymbol{\xi}_I - \boldsymbol{\xi})\boldsymbol{p}^T(\boldsymbol{\xi}_I - \boldsymbol{\xi}) \tag{30}$$

Substituting Eq. (29) back into Eq. (22), the expression of meshfree shape function can be written as:

$$\Psi_I(\boldsymbol{\xi}) = \boldsymbol{p}^T(\boldsymbol{\xi}_I - \boldsymbol{\xi})\boldsymbol{A}^{-1}(\boldsymbol{\xi})\boldsymbol{p}(\boldsymbol{0})\phi(\boldsymbol{\xi}_I - \boldsymbol{\xi}) \tag{31}$$

3.2. Reproducing kernel gradient smoothing approximation for effective stress and strain

In Galerkin meshfree formulation, the mid-plane of thin shell Ω is split by a set of integration cells Ω_C's, $\cup_{C=1}^{n_e}\Omega_C \approx \Omega$, as shown in Fig. 2. With the inspiration of reproducing kernel smoothing framework, the Cartesian and covariant derivatives of displacement, $\boldsymbol{v}_{,\alpha}$ and $-\boldsymbol{v}_{,\alpha}|_\beta$, in strains $\varepsilon_{\alpha\beta}$, $\kappa_{\alpha\beta}$ are approximated by $(p-1)$-th order polynomials in each integration cells. In integration cell Ω_C, the approximated derivatives and strains denoted by $\boldsymbol{v}^h_{,\alpha}$, $\varepsilon^h_{\alpha\beta}$ and $-\boldsymbol{v}^h_{,\alpha}|_\beta$, $\kappa^h_{\alpha\beta}$ can be expressed by:

$$\boldsymbol{v}^h_{,\alpha}(\boldsymbol{\xi}) = \boldsymbol{q}^T(\boldsymbol{\xi})\boldsymbol{d}^\varepsilon_\alpha, \quad \varepsilon^h_{\alpha\beta}(\boldsymbol{\xi}) = \boldsymbol{q}^T(\boldsymbol{\xi})\frac{1}{2}(\boldsymbol{a}_\alpha \cdot \boldsymbol{d}^\varepsilon_\beta + \boldsymbol{a}_\beta \cdot \boldsymbol{d}^\varepsilon_\alpha) \tag{32}$$

$$-\boldsymbol{v}^h_{,\alpha}|_\beta(\boldsymbol{\xi}) = \boldsymbol{q}^T(\boldsymbol{\xi})\boldsymbol{d}^\kappa_{\alpha\beta}, \quad \kappa^h_{\alpha\beta}(\boldsymbol{\xi}) = \boldsymbol{q}^T(\boldsymbol{\xi})\boldsymbol{a}_3 \cdot \boldsymbol{d}^\kappa_{\alpha\beta} \tag{33}$$

where $\boldsymbol{q}$ is the linear polynomial vector and has the following form:

$$\boldsymbol{q} = \{1,\ \xi^1,\ \xi^2\}^T \tag{34}$$

and the $\boldsymbol{d}^\varepsilon_\alpha$, $\boldsymbol{d}^\kappa_{\alpha\beta}$ are the corresponding coefficient vector tensors. For the conciseness, the mixed usage of tensor and vector is introduced in this study. For instance, the component of coefficient tensor vector $\boldsymbol{d}^\varepsilon_{\alpha I}$, $\boldsymbol{d}^\varepsilon_\alpha = \{\boldsymbol{d}^\varepsilon_{\alpha I}\}$, is a three dimensional tensor, $\dim \boldsymbol{d}^\varepsilon_{\alpha I} = \dim \boldsymbol{v}$.

To satisfy the integration constraint of thin shell problem, the approximated stresses $N^{\alpha\beta h}$, $M^{\alpha\beta h}$ were assumed to have a comparable form to strains, and yields:

$$N^{\alpha\beta h}(\boldsymbol{\xi}) = \boldsymbol{q}^T(\boldsymbol{\xi})\boldsymbol{a}^\alpha \cdot \boldsymbol{d}^\beta_N, \quad \boldsymbol{a}_\alpha N^{\alpha\beta h}(\boldsymbol{\xi}) = \boldsymbol{q}^T(\boldsymbol{\xi})\boldsymbol{d}^\beta_N \tag{35}$$

$$M^{\alpha\beta h}(\boldsymbol{\xi}) = \boldsymbol{q}^T(\boldsymbol{\xi})\boldsymbol{a}_3 \cdot \boldsymbol{d}^{\alpha\beta}_M, \quad \boldsymbol{a}_3 M^{\alpha\beta h}(\boldsymbol{\xi}) = \boldsymbol{q}^T(\boldsymbol{\xi})\boldsymbol{d}^{\alpha\beta}_M \tag{36}$$

substituting the approximations of Eqs. (22), (32), (33), (35), (36) into Eqs. (21c), (21d) can express $\boldsymbol{d}^\varepsilon_\beta$ and $\boldsymbol{d}^\kappa_{\alpha\beta}$ by $\boldsymbol{d}$ as:

$$\boldsymbol{d}^\varepsilon_\beta = \boldsymbol{G}^{-1}\left(\sum_{I=1}^{n_p}(\tilde{\boldsymbol{g}}_{\beta I} - \bar{\boldsymbol{g}}_{\beta I})\boldsymbol{d}_I + \hat{\boldsymbol{g}}_\beta\right) \tag{37}$$

$$\boldsymbol{d}^\kappa_{\alpha\beta} = \boldsymbol{G}^{-1}\left(\sum_{I=1}^{n_p}(\tilde{\boldsymbol{g}}_{\alpha\beta I} - \bar{\boldsymbol{g}}_{\alpha\beta I})\boldsymbol{d}_I + \hat{\boldsymbol{g}}_{\alpha\beta}\right) \tag{38}$$

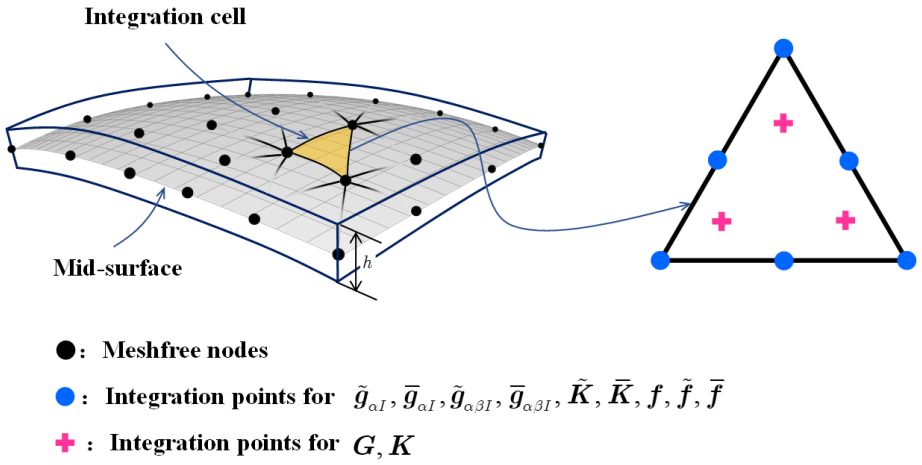

Figure 2: Integration scheme for Hu-Washizu weak form.

with

$$\boldsymbol{G} = \int_{\Omega_C} \boldsymbol{q}^T \boldsymbol{q} d\Omega \tag{39}$$

$$\tilde{\boldsymbol{g}}_{\beta I} = \int_{\Gamma_C} \Psi_I \boldsymbol{q} n_\beta d\Gamma - \int_{\Omega_C} \Psi_I \boldsymbol{q}_{|\beta} d\Omega \tag{40a}$$

$$\bar{\boldsymbol{g}}_{\beta I} = \int_{\Gamma_C \cap \Gamma_v} \Psi_I \boldsymbol{q} n_\beta d\Gamma \tag{40b}$$

$$\hat{\boldsymbol{g}}_{\beta} = \int_{\Gamma_C \cap \Gamma_v} \boldsymbol{q} n_\beta \bar{\boldsymbol{v}} d\Gamma \tag{40c}$$

$$\begin{aligned} \tilde{\boldsymbol{g}}_{\alpha\beta I} = &\int_{\Gamma_C} \Psi_{I,\gamma} n^\gamma \boldsymbol{q} n_\alpha n_\beta d\Gamma - \int_{\Gamma_C} \Psi_I (\boldsymbol{q}_{|\beta} n_\alpha + (\boldsymbol{q} s_\alpha n_\beta)_{,\gamma} s^\gamma) d\Gamma \\ &+ [[\Psi_I \boldsymbol{q} s_\alpha n_\beta]]_{\boldsymbol{x} \in C_C} - \int_{\Omega_C} \Psi \boldsymbol{q}_{,\alpha|\beta} d\Omega \end{aligned} \tag{41a}$$

$$\begin{aligned} \bar{\boldsymbol{g}}_{\alpha\beta I} = &\int_{\Gamma_C \cap \Gamma_\theta} \Psi_{I,\gamma} n^\gamma \boldsymbol{q} n_\alpha n_\beta d\Gamma - \int_{\Gamma_C \cap \Gamma_v} \Psi_I (\boldsymbol{q}_{|\beta} n_\alpha + (\boldsymbol{q} s_\alpha n_\beta)_{,\gamma} s^\gamma) d\Gamma \\ &+ [[\Psi_I \boldsymbol{q} s_\alpha n_\beta]]_{\boldsymbol{x} \in C_C \cap C_v} \end{aligned} \tag{41b}$$

$$\begin{aligned} \hat{\boldsymbol{g}}_{\alpha\beta} = &\int_{\Gamma_C \cap \Gamma_\theta} \boldsymbol{q} n_\alpha n_\beta \boldsymbol{a}_3 \bar{\theta}_{\boldsymbol{n}} d\Gamma - \int_{\Gamma_C \cap \Gamma_v} (\boldsymbol{q}_{|\beta} n_\alpha + (\boldsymbol{q} s_\alpha n_\beta)_{,\gamma} s^\gamma) \bar{\boldsymbol{v}} d\Gamma \\ &+ [[\boldsymbol{q} s_\alpha n_\beta \bar{\boldsymbol{v}}]]_{\boldsymbol{x} \in C_C \cap C_v} \end{aligned} \tag{41c}$$

where evaluations of $\boldsymbol{q}_{|\beta}$, $\boldsymbol{q}_{,\alpha|\beta}$ are discussed in Appendix A. Further plugging Eqs. (37) and (38) back into Eqs. (32) and (33) respectively gives the final

expression of $\boldsymbol{v}^h_{,\alpha}$, $\varepsilon^h_{\alpha\beta}$ and $-\boldsymbol{v}^h_{,\alpha}|_\beta$, $\boldsymbol{\kappa}^h_{\alpha\beta}$ as:

$$\boldsymbol{v}^h_{,\alpha} = \sum_{I=1}^{n_p}(\tilde{\Psi}_{I,\alpha} - \bar{\Psi}_{I,\alpha})\boldsymbol{d}_I + \boldsymbol{q}^T\boldsymbol{G}^{-1}\hat{\boldsymbol{g}}_\alpha \tag{42a}$$

$$\begin{aligned}\varepsilon^h_{\alpha\beta} &= \sum_{I=1}^{n_p}\frac{1}{2}(\boldsymbol{a}_\alpha\tilde{\Psi}_{I,\beta} + \boldsymbol{a}_\beta\tilde{\Psi}_{I,\alpha})\cdot\boldsymbol{d}_I - \sum_{I=1}^{n_p}\frac{1}{2}(\boldsymbol{a}_\alpha\bar{\Psi}_{I,\beta} + \boldsymbol{a}_\beta\bar{\Psi}_{I,\alpha})\cdot\boldsymbol{d}_I \\ &+ \boldsymbol{q}^T\boldsymbol{G}^{-1}\frac{1}{2}(\boldsymbol{a}_\alpha\cdot\hat{\boldsymbol{g}}_\beta + \boldsymbol{a}_\beta\cdot\hat{\boldsymbol{g}}_\alpha) \\ &= \tilde{\varepsilon}^h_{\alpha\beta} - \bar{\varepsilon}^h_{\alpha\beta} + \hat{\varepsilon}^h_{\alpha\beta}\end{aligned} \tag{42b}$$

$$-\boldsymbol{v}^h_{,\alpha}|_\beta = \sum_{I=1}^{n_p}(\tilde{\Psi}_{I,\alpha\beta} - \bar{\Psi}_{I,\alpha\beta})\boldsymbol{d}_I + \boldsymbol{q}^T\boldsymbol{G}^{-1}\hat{\boldsymbol{g}}_{\alpha\beta} \tag{43a}$$

$$\begin{aligned}\kappa^h_{\alpha\beta} &= \sum_{I=1}^{n_p}\tilde{\Psi}_{I,\alpha\beta}\boldsymbol{a}_3\cdot\boldsymbol{d}_I - \sum_{I=1}^{n_p}\bar{\Psi}_{I,\alpha\beta}\boldsymbol{a}_3\cdot\boldsymbol{d}_I + \boldsymbol{q}^T\boldsymbol{G}^{-1}\boldsymbol{a}_3\cdot\hat{\boldsymbol{g}}_{\alpha\beta} \\ &= \tilde{\kappa}^h_{\alpha\beta} - \bar{\kappa}^h_{\alpha\beta} + \hat{\kappa}^h_{\alpha\beta}\end{aligned} \tag{43b}$$

with

$$\begin{cases}\tilde{\varepsilon}^h_{\alpha\beta} = \sum_{I=1}^{n_p}\frac{1}{2}(\boldsymbol{a}_\alpha\tilde{\Psi}_{I,\beta} + \boldsymbol{a}_\beta\tilde{\Psi}_{I,\alpha})\cdot\boldsymbol{d}_I = \sum_{I=1}^{n_p}\tilde{\boldsymbol{\varepsilon}}_{\alpha\beta I}\cdot\boldsymbol{d}_I \\ \bar{\varepsilon}^h_{\alpha\beta} = \sum_{I=1}^{n_p}\frac{1}{2}(\boldsymbol{a}_\alpha\bar{\Psi}_{I,\beta} + \boldsymbol{a}_\beta\bar{\Psi}_{I,\alpha})\cdot\boldsymbol{d}_I = \sum_{I=1}^{n_p}\bar{\boldsymbol{\varepsilon}}_{\alpha\beta I}\cdot\boldsymbol{d}_I \\ \hat{\varepsilon}^h_{\alpha\beta} = \boldsymbol{q}^T\boldsymbol{G}^{-1}\frac{1}{2}(\boldsymbol{a}_\alpha\cdot\hat{\boldsymbol{g}}_\beta + \boldsymbol{a}_\beta\cdot\hat{\boldsymbol{g}}_\alpha)\end{cases} \tag{44}$$

$$\begin{cases}\tilde{\Psi}_{I,\alpha}(\boldsymbol{\xi}) = \boldsymbol{q}^T(\boldsymbol{\xi})\boldsymbol{G}^{-1}\tilde{\boldsymbol{g}}_{\alpha I} \\ \bar{\Psi}_{I,\alpha}(\boldsymbol{\xi}) = \boldsymbol{q}^T(\boldsymbol{\xi})\boldsymbol{G}^{-1}\bar{\boldsymbol{g}}_{\alpha I} \\ \tilde{\boldsymbol{\varepsilon}}_{\alpha\beta I} = \frac{1}{2}(\boldsymbol{a}_\alpha\tilde{\Psi}_{I,\beta} + \boldsymbol{a}_\beta\tilde{\Psi}_{I,\alpha}) \\ \bar{\boldsymbol{\varepsilon}}_{\alpha\beta I} = \frac{1}{2}(\boldsymbol{a}_\alpha\bar{\Psi}_{I,\beta} + \boldsymbol{a}_\beta\bar{\Psi}_{I,\alpha})\end{cases} \tag{45}$$

$$\begin{cases}\tilde{\kappa}^h_{\alpha\beta} = \sum_{I=1}^{n_p}\tilde{\Psi}_{I,\alpha\beta}\boldsymbol{a}_3\cdot\boldsymbol{d}_I = \sum_{I=1}^{n_p}\tilde{\boldsymbol{\kappa}}_{\alpha\beta I}\cdot\boldsymbol{d}_I \\ \bar{\kappa}^h_{\alpha\beta} = \sum_{I=1}^{n_p}\bar{\Psi}_{I,\alpha\beta}\boldsymbol{a}_3\cdot\boldsymbol{d}_I = \sum_{I=1}^{n_p}\bar{\boldsymbol{\kappa}}_{\alpha\beta I}\cdot\boldsymbol{d}_I \\ \hat{\kappa}^h_{\alpha\beta} = \boldsymbol{q}^T\boldsymbol{G}^{-1}\boldsymbol{a}_3\cdot\hat{\boldsymbol{g}}_{\alpha\beta}\end{cases} \tag{46}$$

$$\begin{cases}\tilde{\Psi}_{I,\alpha\beta}(\boldsymbol{\xi}) = \boldsymbol{q}^T(\boldsymbol{\xi})\boldsymbol{G}^{-1}\tilde{\boldsymbol{g}}_{\alpha\beta I} \\ \bar{\Psi}_{I,\alpha\beta}(\boldsymbol{\xi}) = \boldsymbol{q}^T(\boldsymbol{\xi})\boldsymbol{G}^{-1}\tilde{\boldsymbol{g}}_{\alpha\beta I} \\ \tilde{\boldsymbol{\kappa}}_{\alpha\beta I} = \tilde{\Psi}_{I,\alpha\beta}\boldsymbol{a}_3 \\ \bar{\boldsymbol{\kappa}}_{\alpha\beta I} = \bar{\Psi}_{I,\alpha\beta}\boldsymbol{a}_3\end{cases} \tag{47}$$

It has to be noted that, referring to reproducing kernel gradient smoothing framework [34], $\tilde{\Psi}_{I,\alpha}$, $\tilde{\Psi}_{I,\alpha\beta}$ are actually the first and second order smoothed gradients in curvilinear coordinates.If the right hand side integration constraints for first and second order gradients are $\tilde{\boldsymbol{g}}_{\alpha I}$ and $\tilde{\boldsymbol{g}}_{\alpha\beta I}$, respectively, then this formulation can satisfy the variational consistency for the second order polynomials. It should be mentioned that in curved model, the variational consistency for non-polynomial functions, such as trigonometric functions, should be required for the polynomial solution. Even with high order polynomial variational consistency, the proposed formulation cannot exactly reproduce the solution spanned by the basis functions. However, the accuracy of reproducing kernel smoothed gradients is still superior than the traditional meshfree formulation. The numerical examples in the following section will better demonstrate the precision of the reproducing kernel smoothed gradients.

4. Naturally variational enforcement for essential boundary conditions

4.1. Discrete equilibrium equations

With the approximated effective stresses and strains, the last equation of weak form Eq. (21e) becomes:

$$-\sum_{C=1}^{n_e}\sum_{I=1}^{n_p}\delta\boldsymbol{d}_I\cdot\left((\tilde{\boldsymbol{g}}_{\alpha I}^T-\bar{\boldsymbol{g}}_{\alpha I}^T)\boldsymbol{d}_N^\alpha+(\tilde{\boldsymbol{g}}_{\alpha\beta I}^T-\bar{\boldsymbol{g}}_{\alpha\beta I}^T)\boldsymbol{d}_M^{\alpha\beta}\right)=-\sum_{I=1}^{n_p}\delta\boldsymbol{d}_I\cdot\boldsymbol{f}_I \tag{48}$$

where $\boldsymbol{f}_I$'s denote the components of the traditional force vector:

$$\boldsymbol{f}_I=\int_{\Gamma_t}\Psi_I\bar{\boldsymbol{t}}d\Gamma-\int_{\Gamma_M}\Psi_{I,\gamma}n^\gamma\bar{M}_{\boldsymbol{nn}}d\Gamma+[[\Psi_I\boldsymbol{a}_3\bar{P}]]_{\boldsymbol{x}\in C_P}+\int_\Omega\Psi_I\bar{\boldsymbol{b}}d\Omega \tag{49}$$

The left side of Eq. (48) can be simplified using the following steps. For clarity, the derivation of first term in Eq. (48) taken as an example is given by:

$$\begin{aligned}\sum_{I=1}^{n_p}\delta\boldsymbol{d}_I\cdot\tilde{\boldsymbol{g}}_{\alpha I}^T\boldsymbol{d}_N^\alpha&=\sum_{I=1}^{n_p}\delta\boldsymbol{d}_I\cdot(\boldsymbol{G}^{-1}\tilde{\boldsymbol{g}}_{\alpha I})^T\boldsymbol{G}\boldsymbol{d}_N^\alpha\\&=\int_{\Omega_C}\sum_{I=1}^{n_p}\delta\boldsymbol{d}_I\cdot(\boldsymbol{q}^T\boldsymbol{G}^{-1}\tilde{\boldsymbol{g}}_{\alpha I})\boldsymbol{q}^T\boldsymbol{d}_N^\alpha d\Omega\\&=\int_{\Omega_C}\sum_{I=1}^{n_p}\delta\boldsymbol{d}_I\cdot\boldsymbol{a}_\beta(\boldsymbol{q}^T\boldsymbol{G}^{-1}\tilde{\boldsymbol{g}}_{\alpha I})N^{\alpha\beta h}d\Omega\\&=\int_{\Omega_C}\delta\tilde{\varepsilon}_{\alpha\beta}^hN^{\alpha\beta h}d\Omega\end{aligned} \tag{50}$$

following the above procedure and including the weak form of Eqs. (21a), (21b), the left side of Eq. (48) in Ω_C becomes:

$$
\begin{aligned}
&\sum_{I=1}^{n_p} \delta \boldsymbol{d}_I \cdot \left((\tilde{\boldsymbol{g}}_{\alpha I}^T - \bar{\boldsymbol{g}}_{\alpha I}^T) \boldsymbol{d}_N^{\alpha} + (\tilde{\boldsymbol{g}}_{\alpha\beta I}^T - \bar{\boldsymbol{g}}_{\alpha\beta I}^T) \boldsymbol{d}_M^{\alpha\beta} \right) \\
&= \int_{\Omega_C} \left((\delta\tilde{\varepsilon}_{\alpha\beta}^h - \delta\bar{\varepsilon}_{\alpha\beta}^h) N^{\alpha\beta h} + (\delta\tilde{\kappa}_{\alpha\beta}^h - \delta\bar{\kappa}_{\alpha\beta}^h) M^{\alpha\beta h} \right) d\Omega \\
&= \int_{\Omega_C} (\delta\tilde{\varepsilon}_{\alpha\beta}^h - \delta\bar{\varepsilon}_{\alpha\beta}^h) h C^{\alpha\beta\gamma\eta} \varepsilon_{\gamma\eta}^h + (\delta\tilde{\kappa}_{\alpha\beta}^h - \delta\bar{\kappa}_{\alpha\beta}^h) \frac{h^3}{12} C^{\alpha\beta\gamma\eta} \kappa_{\gamma\eta}^h \\
&= \int_{\Omega_C} \delta\tilde{\varepsilon}_{\alpha\beta}^h h C^{\alpha\beta\gamma\eta} \tilde{\varepsilon}_{\gamma\eta}^h d\Omega + \int_{\Omega_C} \delta\tilde{\kappa}_{\alpha\beta}^h \frac{h^3}{12} C^{\alpha\beta\gamma\eta} \tilde{\kappa}_{\gamma\eta}^h d\Omega \\
&- \int_{\Omega_C} \delta\tilde{\varepsilon}_{\alpha\beta}^h h C^{\alpha\beta\gamma\eta} \bar{\varepsilon}_{\gamma\eta}^h d\Omega - \int_{\Omega_C} \delta\bar{\varepsilon}_{\alpha\beta}^h h C^{\alpha\beta\gamma\eta} \tilde{\varepsilon}_{\gamma\eta}^h d\Omega \\
&- \int_{\Omega_C} \delta\tilde{\kappa}_{\alpha\beta}^h \frac{h^3}{12} C^{\alpha\beta\gamma\eta} \bar{\kappa}_{\gamma\eta}^h d\Omega - \int_{\Omega_C} \delta\bar{\kappa}_{\alpha\beta}^h \frac{h^3}{12} C^{\alpha\beta\gamma\eta} \tilde{\kappa}_{\gamma\eta}^h d\Omega \\
&+ \int_{\Omega_C} \delta\bar{\varepsilon}_{\alpha\beta}^h h C^{\alpha\beta\gamma\eta} \bar{\varepsilon}_{\gamma\eta}^h d\Omega + \int_{\Omega_C} \delta\bar{\kappa}_{\alpha\beta}^h \frac{h^3}{12} C^{\alpha\beta\gamma\eta} \bar{\kappa}_{\gamma\eta}^h d\Omega \\
&+ \int_{\Omega_C} (\delta\tilde{\varepsilon}_{\alpha\beta}^h - \delta\bar{\varepsilon}_{\alpha\beta}^h) h C^{\alpha\beta\gamma\eta} \hat{\varepsilon}_{\gamma\eta}^h d\Omega + \int_{\Omega_C} (\delta\tilde{\kappa}_{\alpha\beta}^h - \delta\bar{\kappa}_{\alpha\beta}^h) \frac{h^3}{12} C^{\alpha\beta\gamma\eta} \hat{\kappa}_{\gamma\eta}^h d\Omega
\end{aligned}
\tag{51}
$$

The complete discrete equilibrium equations can be obtained by further substituting Eqs. (44) and (46) into above equation, respectively:

$$
(\boldsymbol{K} + \tilde{\boldsymbol{K}} + \bar{\boldsymbol{K}}) \boldsymbol{d} = \boldsymbol{f} + \tilde{\boldsymbol{f}} + \bar{\boldsymbol{f}} \tag{52}
$$

where the components of stiffness matrices and force vectors in discrete equilibrium equations can be evaluated as follows:

$$
\boldsymbol{K}_{IJ} = \int_{\Omega} \tilde{\boldsymbol{\varepsilon}}_{\alpha\beta I} h C^{\alpha\beta\gamma\eta} \tilde{\boldsymbol{\varepsilon}}_{\gamma\eta J} d\Omega + \int_{\Omega} \tilde{\boldsymbol{\kappa}}_{\alpha\beta I} \frac{h^3}{12} C^{\alpha\beta\gamma\eta} \tilde{\boldsymbol{\kappa}}_{\gamma\eta J} d\Omega \tag{53}
$$

$$
\begin{aligned}
\tilde{\boldsymbol{K}}_{IJ} = &- \int_{\Gamma_v} (\Psi_I \tilde{\boldsymbol{T}}_{NJ} + \tilde{\boldsymbol{T}}_{NI} \Psi_J) d\Gamma \\
&+ \int_{\Gamma_\theta} (\Psi_{I,\gamma} n^\gamma \boldsymbol{a}_3 \tilde{\boldsymbol{M}}_{\boldsymbol{nn}J} + \boldsymbol{a}_3 \tilde{\boldsymbol{M}}_{\boldsymbol{nn}I} \Psi_{J,\gamma} n^\gamma) d\Gamma \\
&+ ([[\Psi_I \boldsymbol{a}_3 \tilde{\boldsymbol{P}}_J]] + [[\tilde{\boldsymbol{P}}_I \boldsymbol{a}_3 \Psi_J]])_{\boldsymbol{x} \in C_v}
\end{aligned}
\tag{54a}
$$

$$
\tilde{\boldsymbol{f}}_I = - \int_{\Gamma_v} \tilde{\boldsymbol{T}}_{NI} \cdot \bar{\boldsymbol{v}} d\Gamma + \int_{\Gamma_\theta} \tilde{\boldsymbol{M}}_{\boldsymbol{nn}I} \bar{\theta}_{\boldsymbol{n}} d\Gamma + [[\tilde{\boldsymbol{P}}_I \boldsymbol{a}_3 \cdot \bar{\boldsymbol{v}}]]_{\boldsymbol{x} \in C_v} \tag{54b}
$$

$$
\bar{\boldsymbol{K}}_{IJ} = - \int_{\Gamma_v} \bar{\boldsymbol{T}}_{MI} \Psi_J d\Gamma + \int_{\Gamma_\theta} \boldsymbol{a}_3 \bar{\boldsymbol{M}}_{\boldsymbol{nn}I} \Psi_{J,\gamma} n^\gamma d\Gamma + [[\bar{\boldsymbol{P}}_I \boldsymbol{a}_3 \Psi_J]]_{\boldsymbol{x} \in C_v} \tag{55a}
$$

$$
\bar{\boldsymbol{f}}_I = - \int_{\Gamma_v} \bar{\boldsymbol{T}}_{MI} \cdot \bar{\boldsymbol{v}} d\Gamma + \int_{\Gamma_\theta} \bar{\boldsymbol{M}}_{\boldsymbol{nn}I} \bar{\theta}_{\boldsymbol{n}} d\Gamma + [[\bar{\boldsymbol{P}}_I \boldsymbol{a}_3 \cdot \bar{\boldsymbol{v}}]]_{\boldsymbol{x} \in C_v} \tag{55b}
$$

The detailed derivations of Eqs (53)-(55) are listed in the Appendix B. As shown in these equations, Eq. (53) is the conventional stiffness matrix evaluated by smoothed gradients $\tilde{\Psi}_{I,\alpha}$, $\tilde{\Psi}_{I,\alpha}|_\beta$, and the Eqs. (54) and (55) contribute for the enforcement of essential boundary. It should be noticed that, in accordance with reproducing kernel smoothed gradient framework, the integration scheme of Eqs. (53-55) should be aligned with those used in the construction of smoothed gradients. The integration scheme used for the proposed method is shown in Fig. 2, in which the total number of the blue circular integration points has been optimized from a global point of view, aiming to reduce the computation of traditional meshfree shape functions and its first order derivatives. In contrast, for assembly stiffness matrix $\boldsymbol{K}$, the low order Gauss integration rule is suitable to ensure the accuracy due to the inherently variational consistency in the smoothed gradients. The detailed positions and weight of the integration points and the efficiency demonstration of this optimized integration scheme can be found in [34, 40]. Examining Eqs. (54) and (55), closely reveal that the structure of the suggested approach to enforce essential boundary conditions is identical to that of the conventional Nitsche's method, with both having the consistent and stabilized terms. Thus, a review of Nitsche's method and a comparison with the proposed approach will be provided in the next subsection.

4.2. Comparison with Nitsche's method

The Nitsche's method for enforcing essential boundaries can be regarded as a combination of Lagrangian multiplier method and penalty method, in which the Lagrangian multiplier is represented by the approximated displacement. The corresponding total potential energy functional Π_P is given by:

$$\begin{aligned}\Pi_P(\boldsymbol{v}) = &\int_\Omega \frac{1}{2}\varepsilon_{\alpha\beta}N^{\alpha\beta}d\Omega + \int_\Omega \frac{1}{2}\kappa_{\alpha\beta}M^{\alpha\beta}d\Omega \\ &- \int_{\Gamma_t} \boldsymbol{v}\cdot\bar{\boldsymbol{t}}d\Gamma + \int_{\Gamma_M} \boldsymbol{v}_{,\gamma}n^\gamma \boldsymbol{a}_3 M_{\boldsymbol{nn}}d\Gamma + (\boldsymbol{v}\cdot\boldsymbol{a}_3 P)_{\boldsymbol{x}\in C_P} - \int_\Omega \boldsymbol{v}\cdot\bar{\boldsymbol{b}}d\Omega \\ &\underbrace{- \int_{\Gamma_v} \boldsymbol{t}\cdot(\boldsymbol{v}-\bar{\boldsymbol{v}})d\Gamma + \int_{\Gamma_\theta} M_{\boldsymbol{nn}}(\theta_{\boldsymbol{n}}-\bar{\theta}_{\boldsymbol{n}})d\Gamma + (P\boldsymbol{a}_3\cdot(\boldsymbol{v}-\bar{\boldsymbol{v}}))_{\boldsymbol{x}\in C_v}}_{\text{consistent term}} \\ &\underbrace{+ \sum_{i=1}^{3}\frac{\alpha_{vi}}{2}\int_{\Gamma_v}(\boldsymbol{v}\cdot\boldsymbol{a}_i)^2 d\Gamma + \frac{\alpha_\theta}{2}\int_{\Gamma_\theta}\theta_{\boldsymbol{n}}^2 d\Gamma + \frac{\alpha_C}{2}(\boldsymbol{v}\cdot\boldsymbol{a}_3)^2_{\boldsymbol{x}\in C_v}}_{\text{stabilized term}}\end{aligned} \tag{56}$$

where the consistent term generated from the Lagrangian multiplier method contributes to enforce the essential boundary, and meet the variational consistency condition. However, the consistent term can not always ensure the coercivity of stiffness, so the penalty method is introduced to serve as a stabilized term, in which α_{vi} is the experimental artificial parameter to enforce the displacement towards the $\boldsymbol{a}_i$ direction, α_θ and α_C are parameters to enforce rotation and corner deflection, respectively. With a standard variational

argument, the corresponding weak form can be stated as:

$$\begin{aligned}\delta\Pi_P(\boldsymbol{v}) = &\int_\Omega \delta\varepsilon_{\alpha\beta}N^{\alpha\beta}d\Omega + \int_\Omega \delta\kappa_{\alpha\beta}M^{\alpha\beta}d\Omega \\ &- \int_{\Gamma_t} \delta\boldsymbol{v}\cdot\bar{\boldsymbol{t}}d\Gamma + \int_{\Gamma_M} \delta\boldsymbol{v}_{,\gamma}n^\gamma\boldsymbol{a}_3M_{\boldsymbol{nn}}d\Gamma + (\delta\boldsymbol{v}\cdot\boldsymbol{a}_3P)_{\boldsymbol{x}\in C_P} - \int_\Omega \delta\boldsymbol{v}\cdot\bar{\boldsymbol{b}}d\Omega \\ &- \int_{\Gamma_v} \delta\boldsymbol{v}\cdot\boldsymbol{t}d\Gamma + \int_{\Gamma_\theta} \delta\theta_{\boldsymbol{n}}M_{\boldsymbol{nn}}d\Gamma + (\boldsymbol{v}\cdot\boldsymbol{a}_3P)_{\boldsymbol{x}\in C_v} \\ &- \int_{\Gamma_v} \delta\boldsymbol{t}\cdot(\boldsymbol{v}-\bar{\boldsymbol{v}})d\Gamma + \int_{\Gamma_\theta} \delta M_{\boldsymbol{nn}}(\theta_{\boldsymbol{n}}-\bar{\theta}_{\boldsymbol{n}})d\Gamma + (\delta P\boldsymbol{a}_3\cdot(\boldsymbol{v}-\bar{\boldsymbol{v}}))_{\boldsymbol{x}\in C_v} \\ &+ \sum_{i=1}^{3}\alpha_{vi}\int_{\Gamma_v}(\delta\boldsymbol{v}\cdot\boldsymbol{a}_i)(\boldsymbol{a}_i\cdot\boldsymbol{v})d\Gamma + \alpha_\theta\int_{\Gamma_\theta}\delta\theta_{\boldsymbol{n}}\theta_{\boldsymbol{n}}d\Gamma + \alpha_C(\delta\boldsymbol{v}\cdot\boldsymbol{a}_3\ \boldsymbol{a}_3\cdot\boldsymbol{v})_{\boldsymbol{x}\in C_v} \\ &= 0\end{aligned} \tag{57}$$

Upon further invoking the conventional reproducing kernel approximation of Eq. (22), the subsequent discrete equilibrium equations can be obtained:

$$(\boldsymbol{K}+\boldsymbol{K}^c+\boldsymbol{K}^s)\boldsymbol{d} = \boldsymbol{f}+\boldsymbol{f}^c+\boldsymbol{f}^s \tag{58}$$

where the stiffness $\boldsymbol{K}$ is identical with Eq. (53). $\boldsymbol{K}^c$ and $\boldsymbol{K}^s$ are the stiffness matrices for consistent and stabilized terms, respectively, and their components have the following form:

$$\begin{aligned}\boldsymbol{K}^c_{IJ} = &-\int_{\Gamma_v}(\Psi_I\boldsymbol{T}_{NJ}+\boldsymbol{T}_{NI}\Psi_J)d\Gamma \\ &+\int_{\Gamma_\theta}(\Psi_{I,\gamma}n^\gamma\boldsymbol{a}_3\boldsymbol{M}_{\boldsymbol{nn}J}+\boldsymbol{a}_3\boldsymbol{M}_{\boldsymbol{nn}I}\Psi_{J,\gamma}n^\gamma)d\Gamma \\ &+([[\Psi_I\boldsymbol{a}_3\boldsymbol{P}_J]]+[[\boldsymbol{P}_I\boldsymbol{a}_3\Psi_J]])_{\boldsymbol{x}\in C_v}\end{aligned} \tag{59a}$$

$$\boldsymbol{f}^c_I = -\int_{\Gamma_v}\boldsymbol{T}_I\cdot\bar{\boldsymbol{v}}d\Gamma + \int_{\Gamma_\theta}\boldsymbol{M}_{\boldsymbol{nn}I}\bar{\theta}_{\boldsymbol{n}}d\Gamma + [[\boldsymbol{P}_I\boldsymbol{a}_3\cdot\bar{\boldsymbol{v}}]]_{\boldsymbol{x}\in C_v} \tag{59b}$$

$$\boldsymbol{K}^s_{IJ} = \boldsymbol{\alpha}_v\int_{\Gamma_v}\Psi_I\Psi_Jd\Gamma + \alpha_\theta\int_{\Gamma_\theta}\Psi_{I,\eta}n^\eta\boldsymbol{a}_3\boldsymbol{a}_3n^\gamma\Psi_{J,\gamma}d\Gamma + \alpha_C[[\Psi_I\boldsymbol{a}_3\boldsymbol{a}_3\Psi_J]]_{\boldsymbol{x}\in C_v} \tag{60a}$$

$$\boldsymbol{f}^s_I = \boldsymbol{\alpha}_v\int_{\Gamma_v}\Psi_I\bar{\boldsymbol{v}}d\Gamma + \alpha_\theta\int_{\Gamma_\theta}\Psi_{I,\eta}n^\eta\boldsymbol{a}_3\bar{\theta}_{\boldsymbol{n}}d\Gamma + \alpha_C[[\Psi_I\boldsymbol{a}_3\boldsymbol{a}_3\cdot\bar{\boldsymbol{v}}]]_{\boldsymbol{x}\in C_v} \tag{60b}$$

with

$$\boldsymbol{\alpha}_v = \begin{bmatrix}\alpha_{v1} & 0 & 0\\ 0 & \alpha_{v2} & 0\\ 0 & 0 & \alpha_{v3}\end{bmatrix} \tag{61}$$

On comparing with the consistent terms of Eqs. (54) and (59), the expressions were almost identical, the major difference is that the higher order

derivatives of shape functions have been replaced by the smoothed gradients. Owing to the reproducing kernel framework, the construction of the smoothed gradients only concerned about the computation of traditional meshfree shape functions and their first order derivatives, which avoid the costly computation of higher order derivatives. Moreover, the stabilized terms in Eq. (60) employs the penalty method with big enough artificial parameters to ensure the coercivity of stiffness. Besides, the optimal values of these artificial parameters are proportional to the grid size of discrete model that can be represented by the support size in meshfree approximation, where $\alpha_{v\alpha} \propto s^{-1}$, $\alpha_{v3} \propto s^{-3}$, $\alpha_\theta \propto s^{-1}$, $\alpha_C \propto s^{-2}$[38], and $s = \min\{s_{\alpha I}\}$. In contrast, the stabilized term of Eq. (55) naturally exists in its weak form, and can stabilize the result without considering any artificial parameters.

5. Numerical examples

In this section, the suggested method is validated through several examples using the Nitsche's method, the consistent reproducing kernel gradient smoothing integration scheme (RKGSI), and the non-consistent Gauss integration scheme (GI) with penalty method, as well as the proposed Hu-Washizu formulation (HW) to enforce the necessary boundary conditions. A normalized support size of 2.5 is used for all the considered methods to ensure the requirement of quadratic base meshfree approximation. To eliminate the influence of integration error, the Gauss integration scheme uses 6 Gauss points for domain integration and 3 points for boundary integration, so as to maintain the same integration accuracy between domain and boundaries. Moreover, the number of integration points are identical between the Gauss and RKGSI schemes. The error estimates of displacement (L_2-Error) and energy (H_e-Error) is used here:

$$
\begin{aligned}
L_2\text{-Error} &= \frac{\sqrt{\int_\Omega (\boldsymbol{v}-\boldsymbol{v}^h)\cdot(\boldsymbol{v}-\boldsymbol{v}^h)d\Omega}}{\sqrt{\boldsymbol{v}\cdot\boldsymbol{v}}} \\
H_e\text{-Error} &= \frac{\sqrt{\int_\Omega \left((\varepsilon_{\alpha\beta}-\varepsilon^h_{\alpha\beta})(N^{\alpha\beta}-N^{\alpha\beta h})+\int_\Omega(\kappa_{\alpha\beta}-\kappa^h_{\alpha\beta})(M^{\alpha\beta}-M^{\alpha\beta h})\right)d\Omega}}{\sqrt{\int_\Omega(\varepsilon_{\alpha\beta}N^{\alpha\beta}+\kappa_{\alpha\beta}M^{\alpha\beta})d\Omega}}
\end{aligned}
\tag{62}
$$

5.1. Patch tests

The linear and quadratic patch tests for flat and curved thin shells are firstly studied to verify the variational consistency of the proposed method. As shown in Fig. 3, the flat and curved models are depicted by an identical parametric domain $\Omega=(0,1)\otimes(0,1)$, where the cylindrical coordinate system with radius $R=1$, thickness $h=0.05$ is employed to describe the curved model, and the whole domain Ω is discretized by the 165 meshfree nodes. The Young's modulus and Poisson's ratio of thin shell are set to $E=1$, $\nu=0$. The artificial parameters of $\alpha_v=10^5\times E$, $\alpha_\theta=10^3\times E$, $\alpha_C=10^5\times E$ and $\alpha_v=10^9\times E, \alpha_\theta=10^9\times E, \alpha_C=10^9\times E$ were adopted in Nitsche's- and penalty- method, respectively. All the boundaries are enforced as essential boundary conditions with the following manufactured exact solution:

$$
\boldsymbol{v}=\begin{Bmatrix}(\xi^1+2\xi^2)^n\\(3\xi^1+4\xi^2)^n\\(5\xi^1+6\xi^2)^n\end{Bmatrix},\quad n=\begin{cases}1 & \text{Linear patch test}\\ 2 & \text{Quadratic patch test}\end{cases}
\tag{63}
$$

Table 1 lists the L_2- and H_e-Error results of patch test with flat model, where the RKGSI scheme with variational consistent essential boundary enforcement, i.e. RKGSI-Nitsche and RKGSI-HW, can pass the linear and quadratic patch test. In contrast, the RKGSI-Penalty cannot pass the patch test since the Penalty method is unable to ensure the variational consistency. Due to the loss of variational consistency condition, even with the Nitsche's method, Gauss

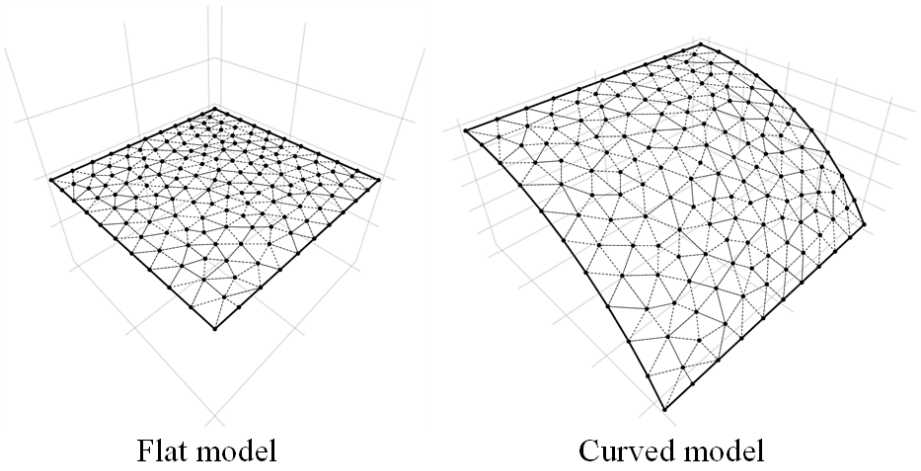

Figure 3: Meshfree discretization for patch test

meshfree formulations show noticeable errors. Table 2 shows the results for curved model, which indicated that all the considered methods cannot pass the patch test. This is mainly because the proposed smoothed gradient of Eqs. (35) and (36) could not exactly reproduce the non-polynomial membrane and bending stresses. On the other hand, the RKGSI-HW and RKGSI-Nitsche methods provide better accuracy compared to the other approaches due to the fulfillment of first second-order variational consistency. Even only with local variational consistency, the RKGSI-Penalty obtained a better result than the traditional Gauss scheme. Meanwhile, the bending moment contours of M^{12} are listed in Fig. 4, which further verify that the proposed method provided a satisfactory result compared to the exact solution. Contrarily, both the RKGSI-Penalty and the conventional Gauss meshree formulations observed errors.

Table 1: Results of patch test for flat model.

	Linear patch test		Quadratic patch test	
	L_2-Error	H_e-Error	L_2-Error	H_e-Error
GI-Penalty	1.41E-04	4.62E-03	1.97E-03	7.17E-03
GI-Nitsche	1.73E-04	5.61E-03	1.85E-03	7.76E-03
RKGSI-Penalty	5.04E-09	1.02E-07	3.01E-09	3.41E-08
RKGSI-Nitsche	9.75E-12	8.98E-11	1.29E-12	1.06E-12
RKGSI-HR	6.15E-13	6.91E-12	7.51E-13	8.36E-12

5.2. Scordelis-Lo roof

This example considers the classical Scordelis-Lo roof problem, as depicted in Fig. 5. The cylindrical roof has dimensions $R = 25$, $L = 50$, $h = 0.25$,

Table 2: Results of patch test for cylindrical model.

	Linear patch test		Quadratic patch test	
	L_2-Error	H_e-Error	L_2-Error	H_e-Error
GI-Penalty	1.75E-04	4.50E-03	1.08E-03	5.83E-03
GI-Nitsche	1.77E-04	5.36E-03	1.07E-03	6.33E-03
RKGSI-Penalty	8.59E-05	9.11E-04	4.28E-04	2.08E-03
RKGSI-Nitsche	1.27E-05	5.32E-05	1.88E-05	5.6E-04
RKGSI-HR	1.43E-05	1.60E-04	2.93E-05	2.85E-04

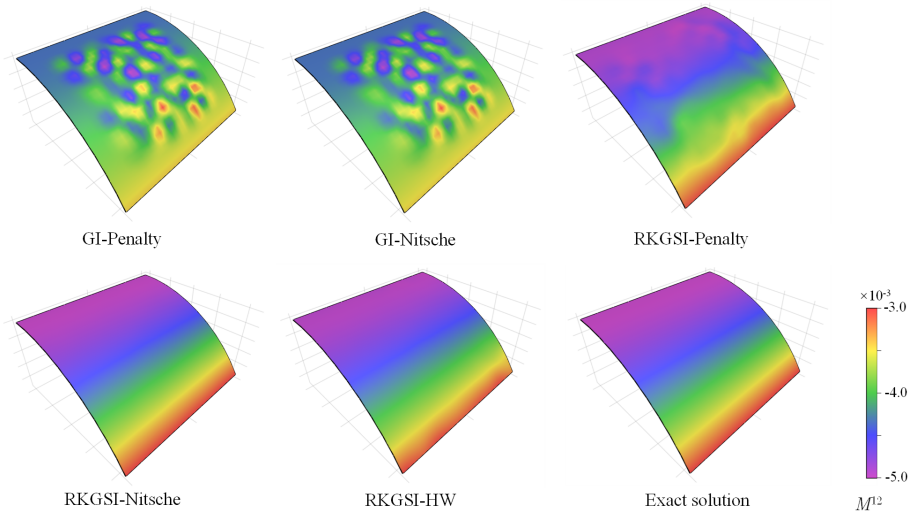

Figure 4: Contour plots of M^{12} for curved shell patch test.

Young's modulus $E = 4.32 \times 10^8$ and Poisson's ratio $\nu = 0.0$. The entire roof is subjected to a uniform body force of $b_z = -90$, with the straight edges remaining free and the curved edges are enforced by $v_x = v_z = 0$.

Due to the symmetry, only a quadrant of the model is considered for meshfree analysis, which is discretized by the 11×16, 13×20, 17×24 and 19×28 meshfree nodes, as listed in Fig. 6. The comparison of the displacement in $z-$direction at node A, v_{A3}, is used as the investigated quantity, with the reference value -0.3006 given by [9]. Firstly, Fig. 7 presents a sensitivity study for the artificial parameters of α_{vi}'s and α_θ's in the RKGSI meshfree formulations with the Nitsche's- and penalty- method, where all the parameters are scaled by the support size as, $\alpha_{v\alpha} = s^{-1}\bar{\alpha}_v$, $\alpha_{v3} = s^{-3}\bar{\alpha}_v$ and $\alpha_\theta = s^{-1}\bar{\alpha}_\theta$. For a better comparison, the result of the proposed RKGSI-HW is also listed in this figure. The results of Fig. 7 revealed, that Nitsche's method observed less artificial sensitivity. However, both the methods cannot trivially determine the optimal values of the artificial parameters. The optimal artificial parameters from Fig.

7 are adopted for the convergence study in Fig. 8. The convergence result showed that the RKGSI method get satisfactory results while the traditional Gauss methods demonstrated noticeable errors.

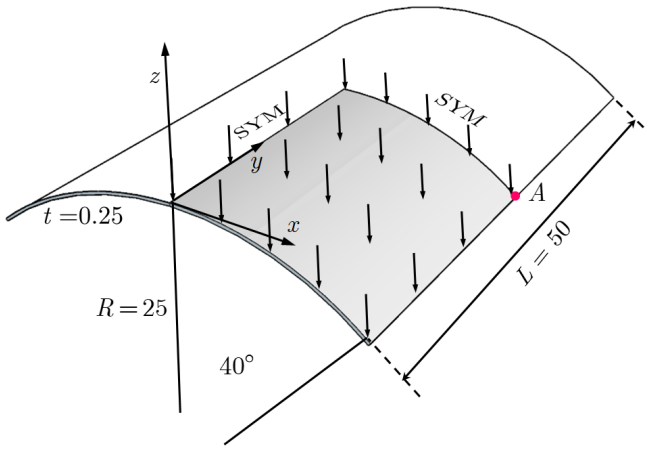

Figure 5: Description of Scordelis-Lo roof problem.

5.3. Pinched Hemispherical shell

Consider the hemispherical shell shown in Fig. 9, which is loaded at four points $P = \pm 2$ at 90° interval at its bottom. The hemispherical shell has a radius $R = 10$, thickness $h = 0.04$, Young's modulus $E = 6.825 \times 10^7$ and Poisson's ratio $\nu = 0.3$.

Due to symmetry, only quadrant model, where the 16×16, 24×24, 32×32 and 40×40 meshfree nodes have been discretized as shown in Fig. (10), were considered. The quantity under investigation for convergence is the displacement at x-direction on point A, $v_{A1} = 0.094$ [41]. Fig. 11 displays the corresponding convergence results, indicating the RKGSI scheme performed significantly better compared to the GI meshfree formulation. Meanwhile, the efficiency comparison for this problem is also shown in Fig. 12, in which the CPU time for assembly and calculation of shape functions are considered. Fig. 12(a) indicates that the RKGSI scheme observed high efficiency in assembly. This is due to the variational inconsistent Gauss meshfree formulation which require more Gaussian points to get satisfactory results. Fig. 12(b) lists the CPU time spent on enforcing essential boundary conditions for the penalty method, Nitsche's method and proposed HW method. The results highlighted that the proposed HW method consumed comparable CPU time in assembly compared to Nitsche's method. However, less time was spent to calculate the shape functions. Since both the HW method and penalty method were developed considering the shape functions first order derivatives. For this reason, both the methods shared an almost identical time in computing the shape functions.

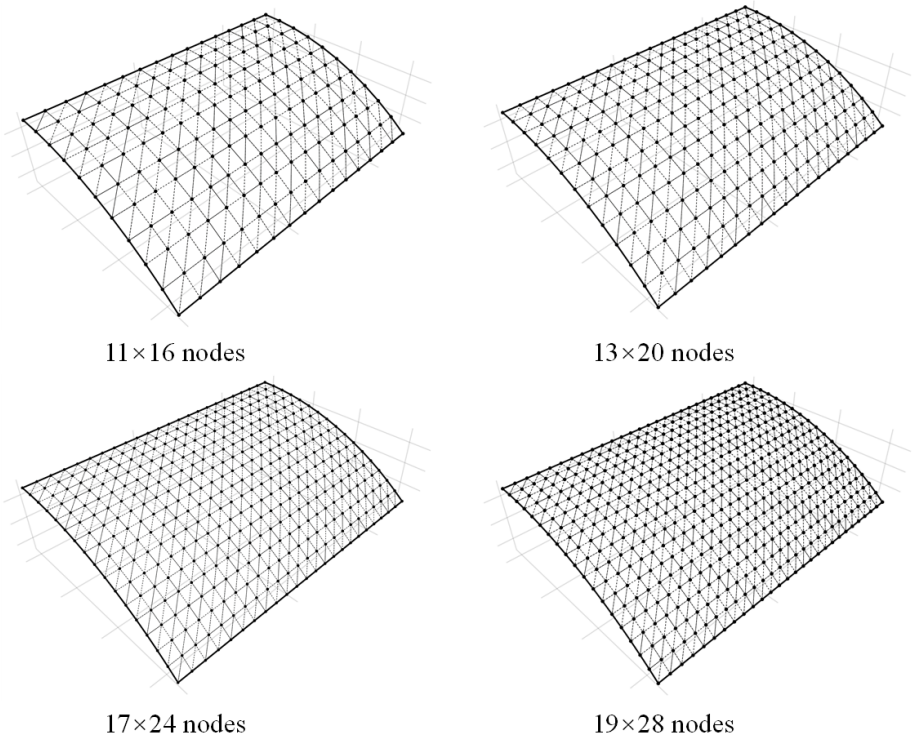

Figure 6: Meshfree discretizations for Scordelis-Lo roof problem.

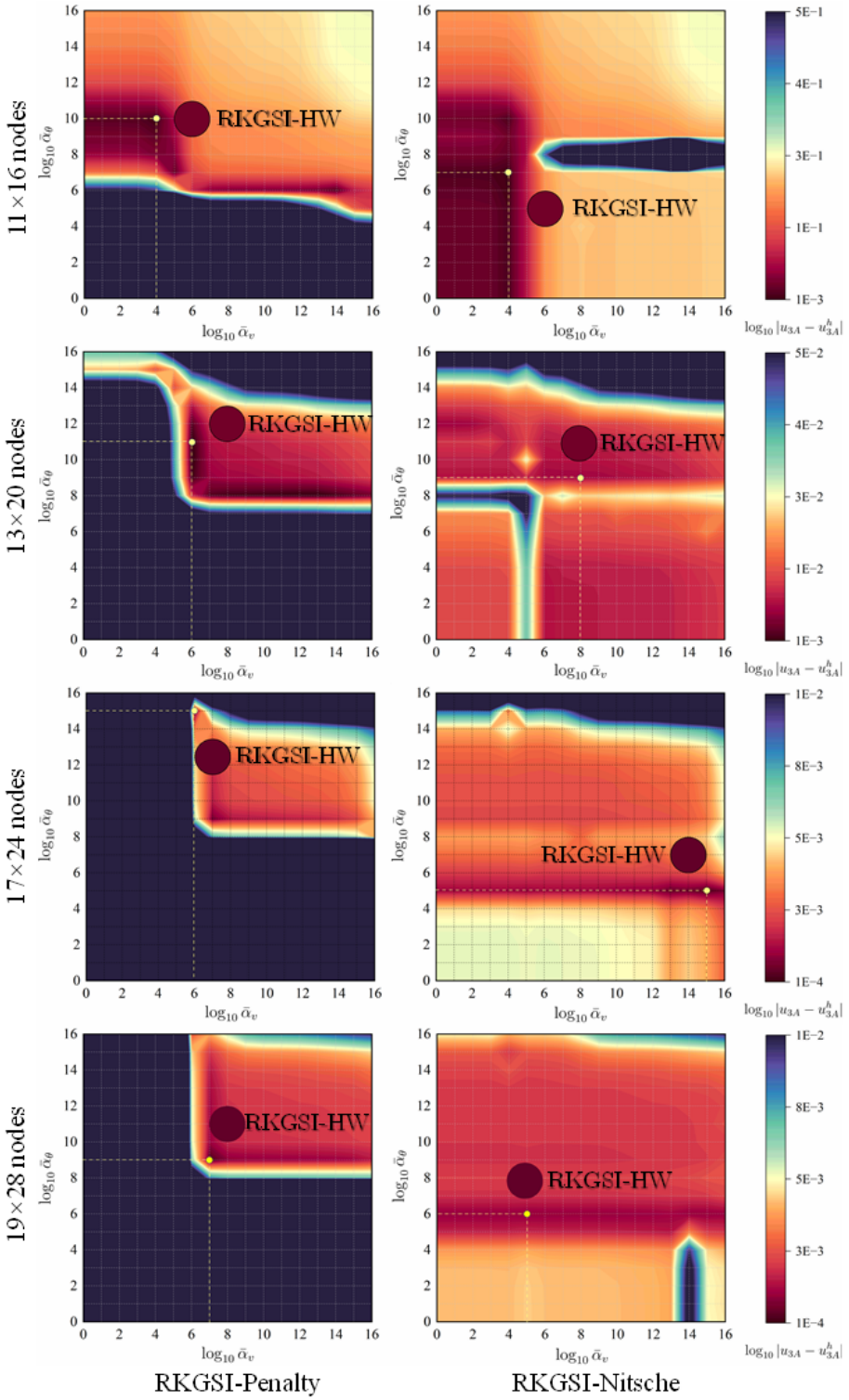

Figure 7: Sensitivity comparison of α_v and α_θ for Scordelis-Lo problem.

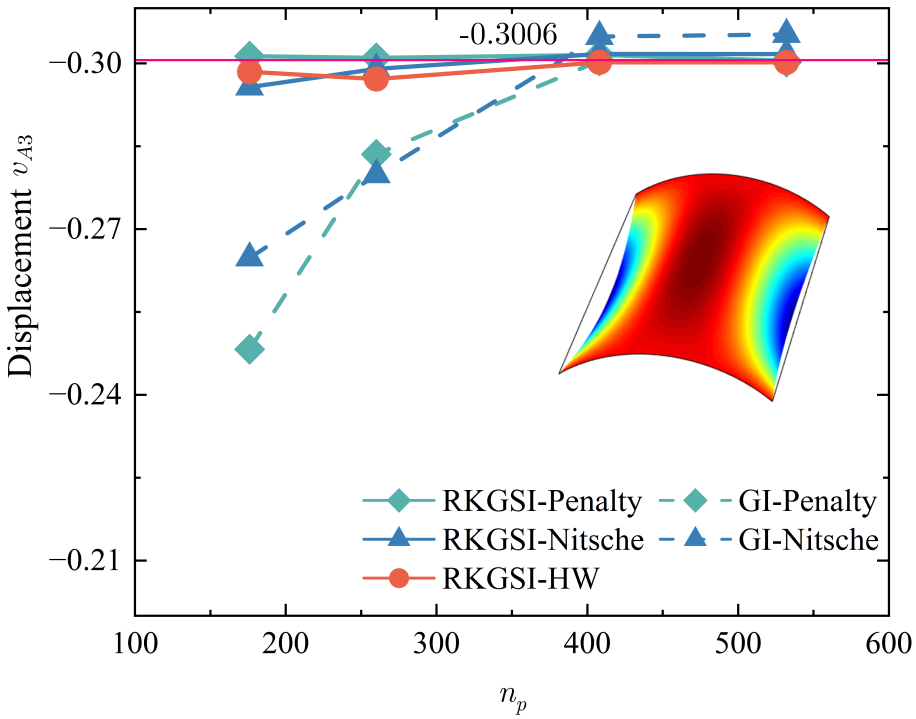

Figure 8: Displacement convergence for Scordelis-Lo roof problem.

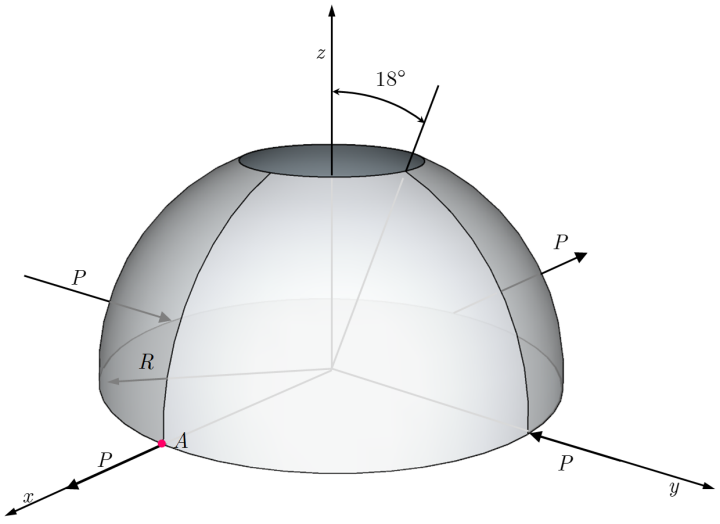

Figure 9: Description of pinched hemispherical shell problem.

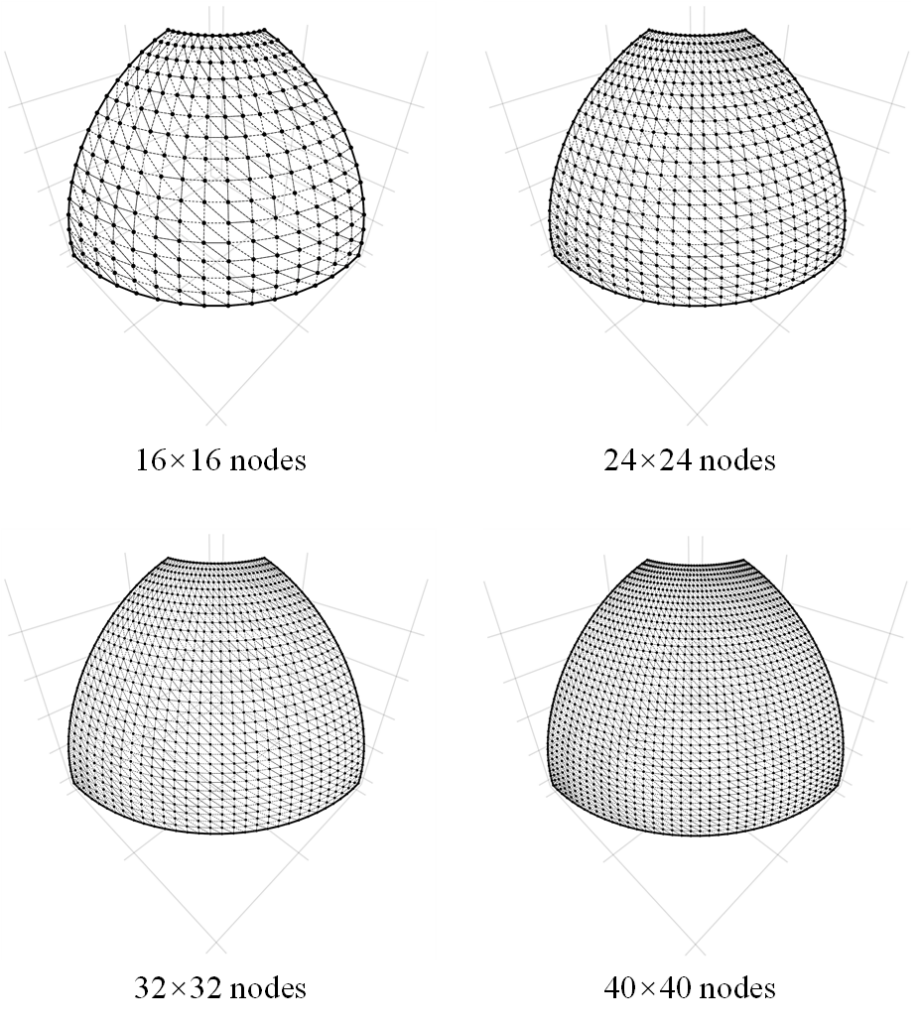

Figure 10: Meshfree discretizations for pinched hemispherical shell problem.

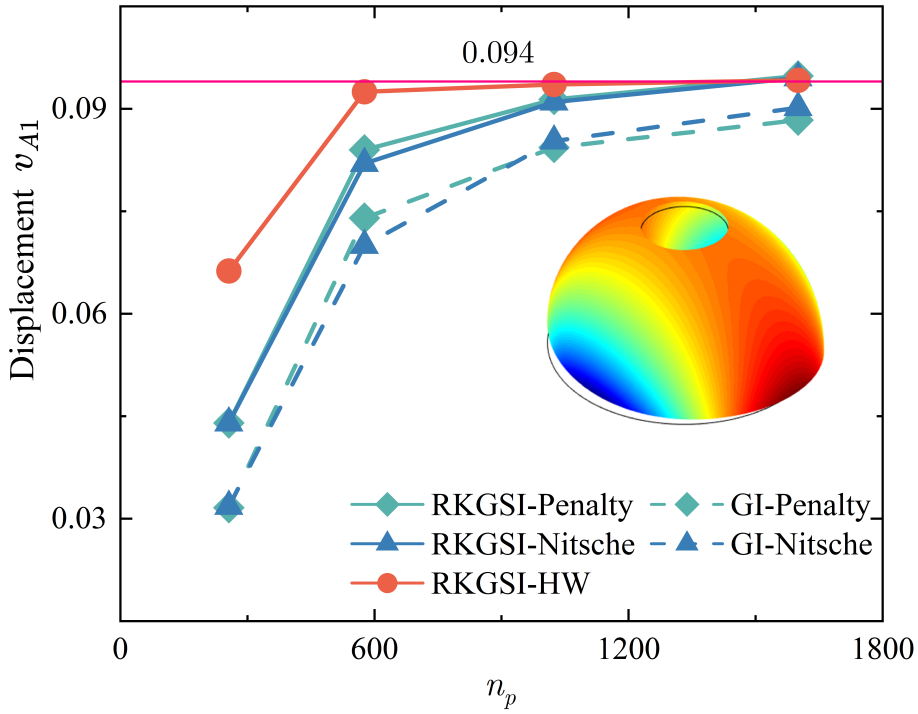

Figure 11: Displacement convergence for pinched hemispherical shell problem.

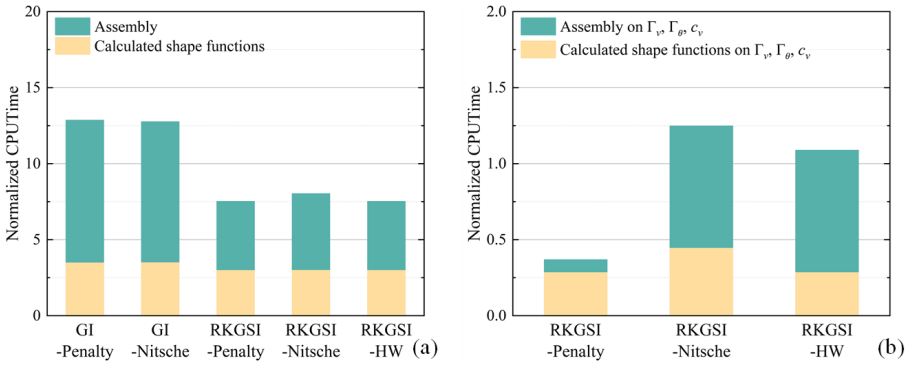

Figure 12: Efficiency comparison for pinched hemispherical shell problem: (a) Whole domain; (b) Essential boundaries

6. Conclusion

In this study, an efficient and quasi-consistent meshfree thin shell formulation was presented to naturally enforce the essential boundary conditions. Mixed formulation with the Hu-Washizu principle weak form is adopted, where the traditional meshfree shape functions discretized the displacement, and the strains and stresses were expressed by the reproducing kernel smoothed gradients and the covariant bases, respectively. The smoothed gradient naturally embedded the first second-order integration constraints and has a quasi variational consistency for the curved models in each integration cell. Owing to the Hu-Washizu variational principle, the essential boundary condition enforcement has a similar form with the conventional Nitsche's method; both have consistent and stabilized terms. The costly high order derivatives in the Nitsche's consistent term have been replaced by the smoothed gradients, which improved the computational speed due to the reproducing kernel gradient smoothing framework. Furthermore, the stabilized term naturally existed in the Hu-Washizu weak form, and the artificial parameter needed in Nitsche's stabilized term has vanished, which can automatically maintain the coercivity for the stiffness matrix. Based on general reproducing kernel gradient smoothing framework, the proposed methodology can be trivially extended to high order basis meshfree formulation. The numerical results demonstrated that the proposed Hu-Washizu quasi-consistent meshfree thin shell formulation showed excellent accuracy, efficiency, and stability.

Acknowledgment

The support of this work by the National Natural Science Foundation of China (12102138, 52350410467) and the Natural Science Foundation of Fujian Province of China (2023J01108, 2022J05056) is gratefully acknowledged.

Appendix A. Green's theorems for in-plane vector

This Appendix discusses two kinds of Green's theorems used for the development of the proposed meshfree method. For an arbitrary vectors v^α and a scalar function f, with Green's theorem for in-plane vector, the first Green's theorem is listed as follows [38]:

$$\begin{aligned}\int_\Omega f_{,\alpha} v^\alpha d\Omega &= \int_\Gamma f v^\alpha n_\alpha d\Gamma - \int_\Omega f(v^\alpha_{,\alpha} + \Gamma^\beta_{\beta\alpha} v^\alpha) d\Omega \\ &= \int_\Gamma f v^\alpha n_\alpha d\Gamma - \int_\Omega f v^\alpha|_\alpha d\Omega\end{aligned} \tag{A.1}$$

where $\Gamma^\gamma_{\alpha\beta} = \boldsymbol{a}_{\alpha,\beta} \cdot \boldsymbol{a}^\gamma$ denotes the Christoffel symbol of the second kind. $v^\alpha|_\alpha$ can be represented as the in-plane covariant derivative of the vector v^α:

$$v^\alpha|_\alpha = v^\alpha_{,\alpha} + \Gamma^\beta_{\beta\alpha} v^\alpha \tag{A.2}$$

The second Green's theorem is established with a mixed form of second order derivative. Let $A^{\alpha\beta}$ can be an arbitrary symmetric second order tensor, the Green's theorem yields [38]:

$$\begin{aligned}\int_\Omega f_{,\alpha}|_\beta A^{\alpha\beta} d\Omega =& \int_\Gamma f_{,\gamma} n^\gamma A^{\alpha\beta} n_\alpha n_\beta d\Gamma - \int_\Gamma f(A^{\alpha\beta} s_\alpha n_\beta)_{,\gamma} s^\gamma d\Gamma + [[f A^{\alpha\beta} s_\alpha n_\beta]]_{\boldsymbol{x}\in C} \\ &- \int_\Gamma f(A^{\alpha\beta}_{,\beta} n_\alpha + \Gamma^\gamma_{\alpha\beta} A^{\alpha\beta} n_\gamma + \Gamma^\gamma_{\gamma\beta} A^{\alpha\beta} n_\alpha) d\Gamma \\ &+ \int_\Omega f \begin{pmatrix} \Gamma^\gamma_{\alpha\beta,\gamma} A^{\alpha\beta} + \Gamma^\gamma_{\alpha\beta} A^{\alpha\beta}_{,\gamma} + \Gamma^\eta_{\eta\gamma} \Gamma^\gamma_{\alpha\beta} A^{\alpha\beta} \\ + A^{\alpha\beta}_{,\alpha\beta} + \Gamma^\gamma_{\gamma\beta,\alpha} A^{\alpha\beta} + 2\Gamma^\gamma_{\gamma\alpha} A^{\alpha\beta}_{,\beta} + \Gamma^\gamma_{\gamma\alpha} \Gamma^\eta_{\eta\beta} A^{\alpha\beta} \end{pmatrix} d\Omega \\ =& \int_\Gamma f_{,\gamma} n^\gamma A^{\alpha\beta} n_\alpha n_\beta d\Gamma - \int_\Gamma f(A^{\alpha\beta} s_\alpha n_\beta)_{,\gamma} s^\gamma d\Gamma + [[f A^{\alpha\beta} s_\alpha n_\beta]]_{\boldsymbol{x}\in C} \\ &- \int_\Gamma f A^{\alpha\beta}|_\beta n_\alpha d\Gamma + \int_\Omega f A^{\alpha\beta}|_{\alpha\beta} d\Omega\end{aligned} \tag{A.3}$$

with

$$A^{\alpha\beta}|_\beta = A^{\alpha\beta}_{,\beta} + \Gamma^\alpha_{\beta\gamma} A^{\beta\gamma} + \Gamma^\gamma_{\gamma\beta} A^{\alpha\beta} \tag{A.4}$$

$$\begin{aligned}A^{\alpha\beta}|_{\alpha\beta} =& \Gamma^\gamma_{\alpha\beta,\gamma} A^{\alpha\beta} + \Gamma^\gamma_{\alpha\beta} A^{\alpha\beta}_{,\gamma} + \Gamma^\eta_{\eta\gamma} \Gamma^\gamma_{\alpha\beta} A^{\alpha\beta} \\ &+ A^{\alpha\beta}_{,\alpha\beta} + \Gamma^\gamma_{\gamma\beta,\alpha} A^{\alpha\beta} + 2\Gamma^\gamma_{\gamma\alpha} A^{\alpha\beta}_{,\beta} + \Gamma^\gamma_{\gamma\alpha} \Gamma^\eta_{\eta\beta} A^{\alpha\beta}\end{aligned} \tag{A.5}$$

For the sake of brevity, the notion of covariant derivative is extended to a scalar function as:

$$f_{|\alpha} = f_{,\alpha} + \Gamma^\beta_{\beta\alpha} f \tag{A.6}$$

$$f_{|\beta} n_\alpha = f_{,\beta} n_\alpha + \Gamma^\gamma_{\alpha\beta} f n_\gamma + \Gamma^\gamma_{\gamma\beta} f n_\alpha \tag{A.7}$$

$$\begin{aligned}f_{|\alpha\beta} =& \Gamma^\gamma_{\alpha\beta,\gamma} f + \Gamma^\gamma_{\alpha\beta} f_{,\gamma} + \Gamma^\eta_{\eta\gamma} \Gamma^\gamma_{\alpha\beta} f \\ &+ f_{,\alpha\beta} + \Gamma^\gamma_{\gamma\beta,\alpha} f + 2\Gamma^\gamma_{\gamma\alpha} f_{,\beta} + \Gamma^\gamma_{\gamma\alpha} \Gamma^\eta_{\eta\beta} f\end{aligned} \tag{A.8}$$

Appendix B. Derivations for stiffness metrics and force vectors

This Appendix details the derivations of stiffness matrices and force vectors in Eqs. (53)-(55), where the relationships of Eqs. (40), (41), (44) and (46) are used herein. Firstly, the membrane strain terms are considered as follows:

$$\begin{aligned}
&\sum_{C=1}^{n_e}\int_{\Omega_C}\delta\tilde{\varepsilon}^h_{\alpha\beta}hC^{\alpha\beta\gamma\eta}\bar{\varepsilon}^h_{\gamma\eta}d\Omega\\
=&\sum_{C=1}^{n_e}\sum_{I,J=1}^{n_p}\delta\boldsymbol{d}_I\cdot\underbrace{\int_{\Omega_C}\tilde{\boldsymbol{\varepsilon}}_{\alpha\beta I}hC^{\alpha\beta\gamma\eta}\boldsymbol{a}_\gamma\boldsymbol{q}^T d\Omega}_{\tilde{\boldsymbol{g}}_I^{\eta T}}\boldsymbol{G}^{-1}\bar{\boldsymbol{g}}_{\eta J}\cdot\boldsymbol{d}_J\\
=&\sum_{C=1}^{n_e}\sum_{I,J=1}^{n_p}\delta\boldsymbol{d}_I\cdot\int_{\Gamma_C\cap\Gamma_v}\Psi_J\underbrace{\boldsymbol{q}^T\boldsymbol{G}^{-1}\tilde{\boldsymbol{g}}_I^{\alpha}n_\alpha}_{\tilde{\boldsymbol{T}}_{NI}}d\Gamma\cdot\boldsymbol{d}_J\\
=&\sum_{I,J=1}^{n_p}\delta\boldsymbol{d}_I\cdot\int_{\Gamma_v}\tilde{\boldsymbol{T}}_{NI}\Psi_J d\Gamma\cdot\boldsymbol{d}_J
\end{aligned}\tag{B.1}$$

with

$$\tilde{\boldsymbol{g}}_I^{\alpha}=\boldsymbol{q}\boldsymbol{a}_\beta hC^{\alpha\beta\gamma\eta}\tilde{\boldsymbol{\varepsilon}}_{\gamma\eta I}\tag{B.2}$$

$$\tilde{\boldsymbol{T}}_{NI}=\boldsymbol{q}^T\boldsymbol{G}^{-1}\tilde{\boldsymbol{g}}_I^{\alpha}n_\alpha\tag{B.3}$$

Following this path, the bending strain terms can be reorganized by:

$$\begin{aligned}
&\sum_{C=1}^{n_e}\int_{\Omega_C}\delta\tilde{\kappa}^h_{\alpha\beta}\frac{h^3}{12}C^{\alpha\beta\gamma\eta}\bar{\kappa}^h_{\gamma\eta}d\Omega\\
=&\sum_{C=1}^{n_e}\sum_{I,J=1}^{n_p}\delta\boldsymbol{d}_I\cdot\underbrace{\int_{\Omega_C}\tilde{\boldsymbol{\kappa}}_{\alpha\beta I}\frac{h^3}{12}C^{\alpha\beta\gamma\eta}\boldsymbol{a}_3\boldsymbol{q}^T d\Omega}_{\tilde{\boldsymbol{g}}_I^{\gamma\eta T}}\boldsymbol{G}^{-1}\bar{\boldsymbol{g}}_{\gamma\eta J}\cdot\boldsymbol{d}_J\\
=&\sum_{C=1}^{n_e}\sum_{I,J=1}^{n_p}\delta\boldsymbol{d}_I\cdot\begin{pmatrix}\displaystyle\int_{\Gamma_C\cap\Gamma_\theta}\underbrace{\boldsymbol{q}^T\boldsymbol{G}^{-1}\tilde{\boldsymbol{g}}_I^{\alpha\beta}n_\alpha n_\beta}_{\tilde{\boldsymbol{M}}_{\boldsymbol{nn}I}}n^\gamma\Psi_{J,\gamma}d\Gamma\\ -\displaystyle\int_{\Gamma_C\cap\Gamma_v}\underbrace{(\boldsymbol{q}^T_{|\beta}\boldsymbol{G}^{-1}\tilde{\boldsymbol{g}}_I^{\alpha\beta}n_\alpha+(\boldsymbol{q}^T\boldsymbol{G}^{-1}\tilde{\boldsymbol{g}}_I^{\alpha\beta}s_\alpha n_\beta)_{,\gamma}s^\gamma)}_{\tilde{\boldsymbol{T}}_{MI}}\Psi_J d\Gamma\\ +[[\underbrace{\boldsymbol{q}^T\boldsymbol{G}^{-1}\tilde{\boldsymbol{g}}_I^{\alpha\beta}s_\alpha n_\beta}_{\tilde{\boldsymbol{P}}_I\boldsymbol{a}_3}\Psi_J]]_{\boldsymbol{x}\in C_C\cap C_v}\end{pmatrix}\cdot\boldsymbol{d}_J\\
=&\sum_{I,J=1}^{n_p}\delta\boldsymbol{d}_I\cdot(\int_{\Gamma_\theta}\tilde{\boldsymbol{M}}_{\boldsymbol{nn}I}n^\gamma\Psi_{J,\gamma}d\Gamma-\int_{\Gamma_v}\tilde{\boldsymbol{T}}_{MI}\Psi_J d\Gamma+[[\tilde{\boldsymbol{P}}_I\Psi_J]]_{\boldsymbol{x}\in C_v})
\end{aligned}\tag{B.4}$$

with

$$\tilde{\boldsymbol{g}}_I^{\alpha\beta} = \int_{\Omega_C} \boldsymbol{q} \frac{h^3}{12} C^{\alpha\beta\gamma\eta} \boldsymbol{a}_3 \tilde{\boldsymbol{\kappa}}_{\gamma\eta I} d\Omega \tag{B.5}$$

$$\begin{cases} \tilde{\boldsymbol{M}}_{\boldsymbol{nn}I} = \boldsymbol{q}^T \boldsymbol{G}^{-1} \tilde{\boldsymbol{g}}_I^{\alpha\beta} n_\alpha n_\beta \\ \tilde{\boldsymbol{T}}_{MI} = \boldsymbol{q}_{|\beta}^T \boldsymbol{G}^{-1} \tilde{\boldsymbol{g}}_I^{\alpha\beta} n_\alpha + (\boldsymbol{q}^T \boldsymbol{G}^{-1} \tilde{\boldsymbol{g}}_I^{\alpha\beta} s_\alpha n_\beta)_{,\gamma} s^\gamma \\ \tilde{\boldsymbol{P}}_I = \boldsymbol{q}^T \boldsymbol{G}^{-1} \tilde{\boldsymbol{g}}_I^{\alpha\beta} s_\alpha n_\beta \cdot \boldsymbol{a}_3 \end{cases} \tag{B.6}$$

References

[1] L. H. Donnell, Beams, Plates and Shells, McGraw-Hill, 1976.

[2] S. Ahmad, B. M. Irons, O. C. Zienkiewicz, Analysis of thick and thin shell structures by curved finite elements, International Journal for Numerical Methods in Engineering 2 (1970) 419–451.

[3] T. J. Hughes, The Finite Element Method: Linear Static and Dynamic Finite Element Analysis, Dover Publications, Mineola, New York, 2000.

[4] J. C. Simo, D. D. Fox, On a stress resultant geometrically exact shell model. Part I: Formulation and optimal parametrization, Computer Methods in Applied Mechanics and Engineering 72 (1989) 267–304.

[5] P. Krysl, T. Belytschko, Analysis of thin shells by the Element-Free Galerkin method, International Journal of Solids and Structures 33 (1996) 3057–3080.

[6] D. Millán, A. Rosolen, M. Arroyo, Thin shell analysis from scattered points with maximum-entropy approximants, International Journal for Numerical Methods in Engineering 85 (2011) 723–751.

[7] D. Wang, C. Song, H. Peng, A Circumferentially Enhanced Hermite Reproducing Kernel Meshfree Method for Buckling Analysis of Kirchhoff–Love Cylindrical Shells, International Journal of Structural Stability and Dynamics 15 (2015) 1450090.

[8] M. Behzadinasab, M. Alaydin, N. Trask, Y. Bazilevs, A general-purpose, inelastic, rotation-free Kirchhoff–Love shell formulation for peridynamics, Computer Methods in Applied Mechanics and Engineering 389 (2022) 114422.

[9] J. Kiendl, K. U. Bletzinger, J. Linhard, R. Wüchner, Isogeometric shell analysis with Kirchhoff–Love elements, Computer Methods in Applied Mechanics and Engineering 198 (2009) 3902–3914.

[10] G. R. Liu, Meshfree Methods: Moving Beyond the Finite Element Method, Second Edition, Crc Press, 2009.

[11] J. S. Chen, M. Hillman, S. W. Chi, Meshfree methods: Progress made after 20 Years, Journal of Engineering Mechanics 143 (2017) 04017001.

[12] X. Zhang, Z. Chen, Y. Liu, The Material Point Method: A Continuum-Based Particle Method for Extreme Loading Cases, Academic Press, Oxford, 2017.

[13] P. Suchde, T. Jacquemin, O. Davydov, Point Cloud Generation for Meshfree Methods: An Overview, Archives of Computational Methods in Engineering 30 (2022) 889–915.

[14] L. Wang, M. Hu, Z. Zhong, F. Yang, Stabilized Lagrange Interpolation Collocation Method: A meshfree method incorporating the advantages of finite element method, Computer Methods in Applied Mechanics and Engineering 404 (2023) 115780.

[15] L. Deng, D. Wang, An accuracy analysis framework for meshfree collocation methods with particular emphasis on boundary effects, Computer Methods in Applied Mechanics and Engineering 404 (2023) 115782.

[16] J. Wang, M. Hillman, Upwind reproducing kernel collocation method for convection-dominated problems, Computer Methods in Applied Mechanics and Engineering 420 (2024) 116711.

[17] J. Wang, M. Behzadinasab, W. Li, Y. Bazilevs, A stable formulation of correspondence-based peridynamics with a computational structure of a method using nodal integration, International Journal for Numerical Methods in Engineering (2024) e7465.

[18] T. Belytschko, Y. Y. Lu, L. Gu, Element-free Galerkin methods, International Journal for Numerical Methods in Engineering 37 (1994) 229–256.

[19] W. K. Liu, S. Jun, Y. F. Zhang, Reproducing kernel particle methods, International Journal for Numerical Methods in Fluids 20 (1995) 1081–1106.

[20] S. Fernández-Méndez, A. Huerta, Imposing essential boundary conditions in mesh-free methods, Computer Methods in Applied Mechanics and Engineering 193 (2004) 1257–1275.

[21] X. Li, Error estimates for the moving least-square approximation and the element-free Galerkin method in n-dimensional spaces, Applied Numerical Mathematics 99 (2016) 77–97.

[22] J. Wu, D. Wang, An accuracy analysis of Galerkin meshfree methods accounting for numerical integration, Computer Methods in Applied Mechanics and Engineering 375 (2021) 113631.

[23] J. S. Chen, H. P. Wang, New boundary condition treatments in meshfree computation of contact problems, Computer Methods in Applied Mechanics and Engineering 187 (2000) 441–468.

[24] D. Liu, Y. M. Cheng, The interpolating element-free Galerkin (IEFG) method for three-dimensional potential problems, Engineering Analysis with Boundary Elements 108 (2019) 115–123.

[25] V. Ivannikov, C. Tiago, P. M. Pimenta, On the boundary conditions of the geometrically nonlinear Kirchhoff–Love shell theory, International Journal of Solids and Structures 51 (2014) 3101–3112.

[26] Y. Y. Lu, T. Belytschko, L. Gu, A new implementation of the element free Galerkin method, Computer Methods in Applied Mechanics and Engineering 113 (1994) 397–414.

[27] T. Zhu, S. N. Atluri, A modified collocation method and a penalty formulation for enforcing the essential boundary conditions in the element free Galerkin method, Computational Mechanics 21 (1998) 211–222.

[28] S. Skatulla, C. Sansour, Essential boundary conditions in meshfree methods via a modified variational principle: Applications to shell computations, Computer Assisted Mechanics and Engineering Sciences 15 (2008) 123–142.

[29] Y. Guo, Z. Zou, M. Ruess, Isogeometric multi-patch analyses for mixed thin shells in the framework of non-linear elasticity, Computer Methods in Applied Mechanics and Engineering 380 (2021) 113771.

[30] J. Wang, G. Zhou, M. Hillman, A. Madra, Y. Bazilevs, J. Du, K. Su, Consistent immersed volumetric Nitsche methods for composite analysis, Computer Methods in Applied Mechanics and Engineering 385 (2021) 114042.

[31] J. S. Chen, C. T. Wu, S. Yoon, Y. You, A stabilized conforming nodal integration for Galerkin mesh-free methods, International Journal for Numerical Methods in Engineering 50 (2001) 435–466.

[32] J. S. Chen, M. Hillman, M. Rüter, An arbitrary order variationally consistent integration for Galerkin meshfree methods, International Journal for Numerical Methods in Engineering 95 (2013) 387–418.

[33] Q. Duan, X. Li, H. Zhang, T. Belytschko, Second-order accurate derivatives and integration schemes for meshfree methods, International Journal for Numerical Methods in Engineering 92 (2012) 399–424.

[34] D. Wang, J. Wu, An inherently consistent reproducing kernel gradient smoothing framework toward efficient Galerkin meshfree formulation with explicit quadrature, Computer Methods in Applied Mechanics and Engineering 349 (2019) 628–672.

[35] J. Wang, X. Ren, A consistent projection integration for Galerkin meshfree methods, Computer Methods in Applied Mechanics and Engineering 414 (2023) 116143.

[36] J. Wu, X. Wu, Y. Zhao, D. Wang, A consistent and efficient method for imposing meshfree essential boundary conditions via hellinger-reissner variational principle., Chinese Journal of Theoretical and Applied Mechanics 54 (2022) 3283–3296.

[37] J. Wu, X. Wu, Y. Zhao, D. Wang, A rotation-free Hellinger-Reissner meshfree thin plate formulation naturally accommodating essential boundary conditions, Engineering Analysis with Boundary Elements 154 (2023) 122–140.

[38] J. Benzaken, J. A. Evans, S. F. McCormick, R. Tamstorf, Nitsche's method for linear Kirchhoff–Love shells: Formulation, error analysis, and verification, Computer Methods in Applied Mechanics and Engineering 374 (2021) 113544.

[39] H. Dah-wei, A method for establishing generalized variational principle, Applied Mathematics and Mechanics 6 (1985) 501–509.

[40] H. Du, J. Wu, D. Wang, J. Chen, A unified reproducing kernel gradient smoothing Galerkin meshfree approach to strain gradient elasticity, Computational Mechanics 70 (2022) 73–100.

[41] R. H. Macneal, R. L. Harder, A proposed standard set of problems to test finite element accuracy, Finite Elements in Analysis and Design 1 (1985) 3–20.